SPRINGER BRIEFS IN
ELECTRICAL AND COMPUTER ENGINEERING

Yuanxiong Guo
Yuguang Fang
Pramod P. Khargonekar

Stochastic Optimization for Distributed Energy Resources in Smart Grids

Springer

SpringerBriefs in Electrical and Computer Engineering

More information about this series at http://www.springer.com/series/10059

Yuanxiong Guo • Yuguang Fang
Pramod P. Khargonekar

Stochastic Optimization for Distributed Energy Resources in Smart Grids

Springer

Yuanxiong Guo
Oklahoma State University
Stillwater, OK, USA

Yuguang Fang
University of Florida
Gainesville, FL, USA

Pramod P. Khargonekar
University of California, Irvine
Irvine, CA, USA

ISSN 2191-8112 ISSN 2191-8120 (electronic)
SpringerBriefs in Electrical and Computer Engineering
ISBN 978-3-319-59528-3 ISBN 978-3-319-59529-0 (eBook)
DOI 10.1007/978-3-319-59529-0

Library of Congress Control Number: 2017943523

Printed on acid-free paper

This Springer imprint is published by Springer Nature
The registered company is Springer International Publishing AG
The registered company address is: Gewerbestrasse 11, 6330 Cham, Switzerland

Preface

With the current trend of transforming a centralized power grid into a decentralized one for efficiency, reliability, and environmental reasons, distributed energy resources (DERs), such as rooftop solar panels, wind turbines, inverters, storage devices, electric vehicles, and smart appliances, are increasingly penetrating into the power distribution networks. These DERs are typically located at the customer side and operated for the purpose of supplying all or a portion of the customer's electric loads. They are also capable of injecting power into the transmission/distribution system, creating bidirectional power flows between the customer and the grid. The growth of DERs is driving the grid of the future and would bring tremendous benefits to our society if they can be effectively integrated. However, controlling large numbers of DERs presents a new challenge for operating the power network safely and efficiently. The adverse impacts on power quality of the network associated with high penetration of DERs, especially issues related to power fluctuations caused by intermittent renewable energy sources, have caused great concerns for the distribution network operators. Also, it becomes hard to instantaneously balance supply and demand for ensuring grid stability due to the distributed and uncertain nature of DERs. The goal of this book is to provide a hierarchical architecture for DER management and present stochastic optimization methods for resource management under the architecture. The targeted audiences are researchers interested in stochastic optimization for DER management, in particular graduate students. It is also our hope that this book can be useful as a quick reference to experts.

This book starts with an introduction on DERs and research challenges for managing DERs in smart grids. Then, a novel hierarchical architecture tailored for managing DERs in smart grids is introduced. Under this architecture, approaches are presented to manage DERs at different levels (i.e., home level, neighborhood level, network level) of this architecture. Different objectives and constraints are considered when formulating the problems at different levels. Stochastic optimization methods that are suitable for implementation at each level are described to solve the formulated problems.

Some of the calculations and proofs involved are mathematical and can be safely skipped in first reading. Nevertheless, we decided to include them because they either illustrate useful analytical skills or provide details that are missing in the original papers. Due to the limited time, space, and of course our knowledge and ability, the content of this book is far from extensive. It only includes closely related literature that we are mostly familiar with.

We would like to express our greatest appreciation to Dr. Xuemin (Sherman) Shen for providing us the opportunity of writing this short book for Springer. We are also grateful to all our collaborators and colleagues. Finally, we would like to thank Springer for the support in various aspects in the writing and publishing of this book.

This research work was supported in part by the U.S. National Science Foundation under Grants CNS-1147813, ECCS-1129062, CNS-1239274, and CNS-1343356.

Stillwater, OK, USA — Yuanxiong Guo
Gainesville, FL, USA — Yuguang Fang
Irvine, CA, USA — Pramod P. Khargonekar
April 2017

Contents

Acronyms

CHP	Combined heat and power
CVaR	Conditional value at risk
DER	Distributed energy resource
DG	Distributed generation
ES	Energy storage
FAN	Field area network
HAN	Home area network
LCMA	Lyapunov-based cost minimization algorithm
LSE	Load serving entity
MILP	Mixed integer linear program
PHEV	Plug-in hybrid electric vehicle
PV	Photovoltaics
RES	Renewable energy source
SOC	State of charge
TS	Thermal storage
VaR	Value at risk

Chapter 1
Hierarchical Architecture for Distributed Energy Resource Management

1.1 Introduction to DERs

With the current trend of transforming a centralized power grid into a decentralized one for efficiency, reliability, and environmental reasons, distributed energy resources (DERs), which refer to a range of small-scale and modular devices designed to provide electricity as well as thermal energy, are increasing penetrating into the power distribution networks. Typical examples of DER units include distributed generation (e.g., rooftop solar panels, wind turbines, and diesel generators), distributed storage (e.g., batteries and thermal storage units), and controllable loads (e.g., electric vehicles, air conditioners, and smart appliances) with different capabilities and characteristics. These DERs are typically located at the customer side and operated for the purpose of supplying all or a portion of the customer's electric loads. They are capable of injecting power into the transmission/distribution system, creating bidirectional power flows between the customer and the grid. Such bidirectional power flows would shift the role of customers in the grid from traditional passive consumers into active "prosumers" which both produce and consume energy depending on their local energy requirements. The increasing deployment of DERs is driven by several distinct benefits. Firstly, renewable energy sources can significantly reduce carbon emissions. Secondly, DERs are located close to the demand side, which can improve power quality and system reliability. Additionally, combined heat and power (CHP), also known as co-generation, can locally utilize the waste heat in the process of power conversion and improve the overall efficiency. These three benefits are the key motivations to deploy DERs in power distribution systems [1]. The growth of DERs is driving the grid of the future (i.e., smart grid) and would bring tremendous benefits to our society if they can be effectively integrated.

Y. Guo et al., *Stochastic Optimization for Distributed Energy Resources in Smart Grids*, SpringerBriefs in Electrical and Computer Engineering,
DOI 10.1007/978-3-319-59529-0_1

1.2 Research Challenges for Integrating DERs

However, controlling large numbers of DERs presents a new challenge for operating the power network safely and efficiently. The adverse impacts on power quality of the network associated with high penetration of DERs, especially issues related to power fluctuations caused by intermittent renewable energy sources, have caused great concerns for the distribution network operators [2]. Also, it becomes hard to instantaneously balance supply and demand for ensuring grid stability due to the distributed and uncertain nature of DERs [1, 3]. To fully realize the benefits of DERs without affecting power quality and grid stability, the key is to achieve coordinated management of large numbers of DERs rather than naive statistical averaging of large numbers of uncoordinated random decisions as adopted in the current practice. By leveraging pervasive sensing, communication, computation, and control technologies in emerging smart grids, we could manage the aggregated capabilities of a cluster of DERs so that the cluster appears to the grid as a self-controlled dispatchable entity and therefore can provide valuable resources to the grid. This necessitates the development of innovative approaches to coordinate large numbers of DERs, which is a difficult task mainly due to the following reasons:

- **Resource Uncertainty**. Different from conventional generation technologies, power production of renewable generation, especially from wind and solar sources, depends on meteorological conditions and is highly uncertain. Furthermore, demand response resources from customers whose actions usually depend on many unknown factors add additional uncertainty. With the increased uncertainty brought by DERs, it becomes much more difficult to ensure the instantaneous power balance in the grid, which must be addressed appropriately.
- **Resource Complexity**. DERs are widely distributed and have different characteristics. Storage devices are different in terms of the charging and discharging rates, efficiency, and capacity. Smart loads are different in their flexibilities in decreasing and increasing demand to mitigate energy imbalance in the grid, which are constrained by their intended service requirements. Moreover, the resource availabilities of some DERs such as storage and deferrable loads are highly coupled across time and increase the complexity in managing them. Therefore, flexible and easy-to-adapt models are needed to accurately analyze and mitigate the impacts of DERs on the grid.
- **Lack of Visibility**. Because of the "behind-the-meter" nature of these DERs, the system operator is in short of the situational awareness that is necessary for ensuring power balances economically and reliably. Note that it is unrealistic to assume that the system operator would be able to sense and control every individual DER belonging to the customers themselves due to the extremely high sensing, communication, computation, and control overhead as well as the potential privacy issues. Hence, proper operation methods must be designed to effectively manage these resources.

1.3 A Novel Hierarchical Architecture for DER Management

To achieve coordinated management of large numbers of DERs in a scalable and economic way, we employ a three-level hierarchical architecture as shown in Fig. 1.1 based on the fact that most power distribution network topologies are radial in practice. The main idea behind this architecture is to push intelligence to the edge of the grid. In this architecture, large numbers of DERs are integrated into a three-level hierarchy through advanced sensing, communication, computation, and control capabilities: a set of basic DERs located behind the same smart meter are first integrated into a smart home (home level); a collection of smart homes that are served by the same bus are then integrated into a smart neighborhood (neighborhood level); and a cluster of neighborhoods located at different buses downstream of the same distribution substation are finally integrated into a smart microgrid (microgrid level). Aggregation managers are constructed throughout the hierarchy to use the sensing, communication, computation, and control infrastructure to intelligently manage the aggregated capabilities of resources. The managed aggregation is then transformed into a single dispatchable entity from the perspective of its upper-level manager. Specifically, the lowest level in the hierarchical architecture consists of homes. Each home in the home level is managed by a home energy manager and can represent a residential household, a data center or an office building.

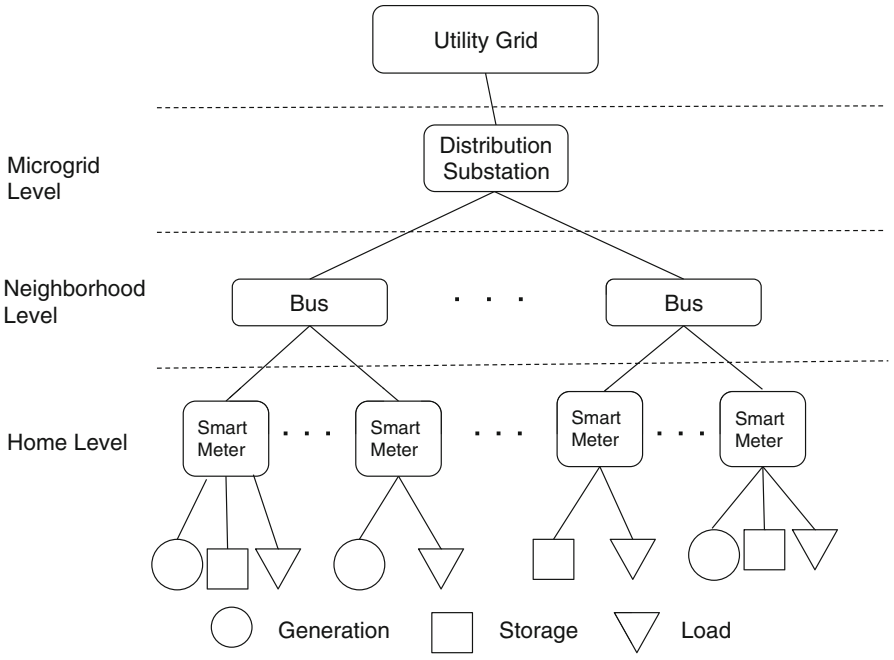

Fig. 1.1 Illustration of the hierarchical architecture

The middle level in the hierarchical architecture is comprised of neighborhoods. Each neighborhood in the neighborhood level is managed by a neighborhood energy manager and could be a neighborhood of residential households or a set of office buildings along the same street. The top level includes multiple neighborhoods connected to a distribution substation forming into a microgrid with a microgrid manager. This hierarchy-based architecture provides higher flexibility for DER integration and greatly reduces the control overhead of the distribution system operator compared to the traditional single-level architecture that requires the operator to monitor and control every single DER.

In this book, we describe effective resource management solutions for integrating DERs under the proposed hierarchical architecture. Novel resource scheduling and optimization algorithms at each level are presented by taking into account its unique features and constraints. Specifically, the rest of this book will be organized into the following three chapters:

- **Chapter 2: Smart Home.** In this chapter, we focus on a single home with DERs such as rooftop solar panels and storage installed on its premise. Considering the uncertainty of resources such as renewable generation and flexible loads, we investigate how to optimally schedule these resources so as to minimize the operation cost or maximize the profit for the home based on stochastic optimization techniques.
- **Chapter 3: Smart Neighborhood.** Considering the connection of multiple homes forming into a neighborhood, in this chapter we investigate coordination schemes for the community manager. Decentralized scheduling algorithms that can incentivize the homes to collaborate and maximize the total benefits of the community are developed.
- **Chapter 4: Smart Microgrid.** Here neighborhoods located at different buses are connected to a distribution substation and form into a microgrid. We investigate the optimal operation schemes for the microgrid in this chapter and present a two-stage stochastic optimization scheme to ensure power balances under uncertainty.

1.4 Related Work

There has been an increasing research interest in distributed energy resources and renewable energy integration during the past few years. Because of page limitation, only a few works are briefly explained here, and some other existing research efforts in this area are referred to in [1, 2, 4–31]. Specifically, for energy management in a single customer, Mohsenian-Rad et al. [11] formulate the optimal control of multiple flexible appliances as a linear program to achieve a desired trade-off between the electricity payment and the waiting time for the operation of each appliance in a residential household, where the customer is subject to a real-time pricing tariff combined with inclining block rates. Kim et al. [14] investigate the problem of causally scheduling power consumption in

real-time pricing environment, which minimizes the expected cost for a single flexible appliance from the residential customer's viewpoint. Both of these studies consider the energy consumption scheduling for a customer who is still a consumer and the case of prosumers needs to be further studied. From the view of multiple customers, Mohsenian-Rad et al. [27] propose a game-theoretical approach to handle the case of multiple residential households in a neighborhood, Li et al. [24] consider the problem of optimal demand response as a convex optimization problem and study the role of dynamic pricing, and Jiang et al. [25] propose a model that integrates two-period electricity markets, renewable generation, and real-time dynamic demand response, and derive the optimal control decisions to optimize the social welfare. Although these studies consider certain features of resource management of prosumer communities, they mostly assume that the uncertain resources can be predicted accurately or propose heuristic algorithms without performance guarantee. In terms of DER networks, the microgrid architecture [32, 33] has been proposed. Under the microgrid architecture, the energy management problem has been extensively studied, including unit commitment [34–39], economic dispatch [40–43], and optimal power flow [44–48]. Since a microgrid is designed to operate in an islanded mode as well as grid connected mode, it can be viewed as a specific aggregation type of DER network. Another related architecture is the virtual power plant [31], which is a managed collection of distributed resources and appears as a traditional generator to the core transmission grid. A virtual power plant can also be viewed as another aggregation type of DER network with the common objective of participating into the electricity market. The energy management problem of virtual power plant has also been investigated in several studies [49–53]. All of these research in microgrids and virtual power plants are related to ours, but they often assume a flat architecture rather than a hierarchical architecture as in the proposed project.

References

1. Nikos Hatziargyriou, Hiroshi Asano, Reza Iravani, and Chris Marnay. Microgrids. *IEEE Power and Energy Magazine*, 5(4):78–94, 2007.
2. Johan Driesen and Farid Katiraei. Design for distributed energy resources. *IEEE Power and Energy Magazine*, 6(3):30–40, 2008.
3. Farid Katiraei, Reza Iravani, Nikos Hatziargyriou, and Aris Dimeas. Microgrids management. *IEEE Power and Energy Magazine*, 6(3):54–65, 2008.
4. A. Ipakchi and F. Albuyeh. Grid of the future. *IEEE Power and Energy Magazine*, 7(2):52–62, 2009.
5. Vijay Vittal. The impact of renewable resources on the performance and reliability of the electricity grid. U.S. National Academy of Engineering, 2010.
6. P.F. Ribeiro, B.K. Johnson, M.L. Crow, A. Arsoy, and Y. Liu. Energy storage systems for advanced power applications. *Proceedings of the IEEE*, 89(12):1744–1756, Dec 2001.
7. B.P. Roberts and C. Sandberg. The role of energy storage in development of smart grids. *Proceedings of the IEEE*, 99(6):1139–1144, Jun 2011.

8. Tony Markel and Andrew Simpson. Plug-in hybrid electric vehicle energy storage system design. In *Advanced Automotive Battery Conference*, Baltimore, MD, May 2006.
9. Miao He, S. Murugesan, and Junshan Zhang. Multiple timescale dispatch and scheduling for stochastic reliability in smart grids with wind generation integration. In *IEEE INFOCOM*, pages 461–465, Shanghai, China, 2011.
10. R.N. Anderson, A. Boulanger, W.B. Powell, and W. Scott. Adaptive stochastic control for the smart grid. *Proceedings of the IEEE*, 99(6):1098–1115, Jun 2011.
11. A.-H. Mohsenian-Rad and A. Leon-Garcia. Optimal residential load control with price prediction in real-time electricity pricing environments. *IEEE Transactions on Smart Grid*, 1(2):120–133, Sep 2010.
12. M.J. Neely, A.S. Tehrani, and A.G. Dimakis. Efficient algorithms for renewable energy allocation to delay tolerant consumers. In *IEEE SmartGridComm*, pages 549–554, Washington, DC, Oct 2010.
13. A. Papavasiliou and S.S. Oren. Supplying renewable energy to deferrable loads: Algorithms and economic analysis. In *IEEE Power and Energy Society General Meeting*, 2010.
14. T. T. Kim and H. V. Poor. Scheduling power consumption with price uncertainty. *IEEE Transactions on Smart Grid*, 2(3):519–527, Sep 2011.
15. Aman Kansal, Jason Hsu, Sadaf Zahedi, and Mani B. Srivastava. Power management in energy harvesting sensor networks. *ACM Transactions on Embedded Computing System*, 6(4):32–38, Sep 2007.
16. O. Ozel, K. Tutuncuoglu, Jing Yang, S. Ulukus, and A. Yener. Resource management for fading wireless channels with energy harvesting nodes. In *IEEE INFOCOM*, pages 456–460, 2011.
17. Shengbo Chen, P. Sinha, N.B. Shroff, and Changhee Joo. Finite-horizon energy allocation and routing scheme in rechargeable sensor networks. In *IEEE INFOCOM*, pages 2273–2281, 2011.
18. M. Gatzianas, L. Georgiadis, and L. Tassiulas. Control of wireless networks with rechargeable batteries. *IEEE Transactions on Wireless Communications*, 9(2):581–593, Feb. 2010.
19. Longbo Huang and Michael J. Neely. Utility optimal scheduling in energy harvesting networks. In *ACM MobiHoc*, 2011.
20. M.K.C. Marwali, H. Ma, S.M. Shahidehpour, and K.H. Abdul-Rahman. Short term generation scheduling in photovoltaic-utility grid with battery storage. *IEEE Transactions on Power Systems*, 13(3):1057–1062, Aug 1998.
21. Ruey-Hsun Liang and Jian-Hao Liao. A fuzzy-optimization approach for generation scheduling with wind and solar energy systems. *IEEE Transactions on Power Systems*, 22(4):1665–1674, Nov 2007.
22. Rahul Urgaonkar, Bhuvan Urgaonkary, Michael J. Neely, and Anand Sivasubramaniam. Optimal power cost management using stored energy in data centers. In *ACM SIGMETRICS*, pages 221–232, 2011.
23. Yuanxiong Guo, Zongrui Ding, Yuguang Fang, and Dapeng Wu. Cutting down electricity cost in internet data centers by using energy storage. In *IEEE GLOBECOM*, 2011.
24. Na Li, Lijun Chen, and Steven H. Low. Optimal demand response based on utility maximization in power networks. In *IEEE Power and Energy Society General Meeting*, 2011.
25. Libin Jiang and Steven H. Low. Multi-period optimal energy procurement and demand response in smart grid with uncertain supply. In *Decision and Control and European Control Conference (CDC-ECC)*, 2011.
26. Eilyan Y. Bitar, Ram Rajagopal, Pramod P. Khargonekar, Kameshwar Poolla, and Pravin Varaiya. Bringing wind energy to market. *IEEE Transactions on Power Systems*, 27(3): 1225–1235, August 2012.
27. A. Mohsenian-Rad, V.W.S. Wong, J. Jatskevich, R. Schober, and A. Leon-Garcia. Autonomous demand-side management based on game-theoretic energy consumption scheduling for the future smart grid. *IEEE Transactions on Smart Grid*, 1(3):320–331, Dec 2010.
28. Yuanxiong Guo, Miao Pan, and Yuguang Fang. Optimal power management of residential customers in the smart grid. *Parallel and Distributed Systems, IEEE Transactions on*, 23(9):1593–1606, Septeneber 2012.

29. P. Palensky and D. Dietrich. Demand side management: Demand response, intelligent energy systems, and smart loads. *IEEE Transactions on Industrial Informatics*, 7(3):381–388, Aug 2011.
30. Hassan Farhangi. The path of the smart grid. *IEEE Power and Energy Magazine*, 8(1): 18–28, 2010.
31. Danny Pudjianto, Charlotte Ramsay, and Goran Strbac. Virtual power plant and system integration of distributed energy resources. *IET Renewable Power Generation*, 1(1):10–16, 2007.
32. Robert H Lasseter. Microgrids. In *IEEE Power Engineering Society Winter Meeting*. IEEE, 2002.
33. R. H. Lasseter. Smart distribution: coupled microgrids. *Proceedings of the IEEE*, 99(6): 1074–1082, 2011.
34. Carlos A Hernandez-Aramburo, Tim C Green, and Nicolas Mugniot. Fuel consumption minimization of a microgrid. *IEEE Transactions on Industry Applications*, 41(3):673–681, 2005.
35. Antonis G Tsikalakis and Nikos D Hatziargyriou. Centralized control for optimizing microgrids operation. In *IEEE Power and Energy Society General Meeting*, 2011.
36. SX Chen, Hoay Beng Gooi, and MingQiang Wang. Sizing of energy storage for microgrids. *IEEE Transactions on Smart Grid*, 3(1):142–151, 2012.
37. Shaghayegh Bahramirad, Wanda Reder, and Amin Khodaei. Reliability-constrained optimal sizing of energy storage system in a microgrid. *IEEE Transactions on Smart Grid*, 3(4): 2056–2062, 2012.
38. Daniel E Olivares, Claudio A Cañizares, and Mehrdad Kazerani. A centralized energy management system for isolated microgrids. *IEEE Transactions on Smart Grid*, 5(4): 1864–1875, 2014.
39. Duong Tung Nguyen and Long Bao Le. Optimal bidding strategy for microgrids considering renewable energy and building thermal dynamics. *IEEE Transactions on Smart Grid*, 5(4):1608–1620, 2014.
40. Xiaohong Guan, Zhanbo Xu, and Qing-Shan Jia. Energy-efficient buildings facilitated by microgrid. *IEEE Transactions on Smart Grid*, 1(3):243–252, 2010.
41. Hao Liang, Bong Jun Choi, Atef Abdrabou, Weihua Zhuang, and Xuemin Sherman Shen. Decentralized economic dispatch in microgrids via heterogeneous wireless networks. *IEEE Journal on Selected Areas in Communications*, 30(6):1061–1074, 2012.
42. Katayoun Rahbar, Jie Xu, and Rui Zhang. Real-time energy storage management for renewable integration in microgrid: An off-line optimization approach. *IEEE Transactions on Smart Grid*, 6(1):124–134, 2015.
43. Ahmed Ouammi, Hanane Dagdougui, Louis Dessaint, and Roberto Sacile. Coordinated model predictive-based power flows control in a cooperative network of smart microgrids. *IEEE Transactions on Smart Grid*, 6(5):2233–2244, 2015.
44. Emiliano Dall'Anese, Hao Zhu, and Georgios B Giannakis. Distributed optimal power flow for smart microgrids. *IEEE Transactions on Smart Grid*, 4(3):1464–1475, 2013.
45. Yoash Levron, Josep M Guerrero, and Yuval Beck. Optimal power flow in microgrids with energy storage. *IEEE Transactions on Power Systems*, 28(3):3226–3234, 2013.
46. Wenbo Shi, Xiaorong Xie, Chi-Cheng Chu, and Rajit Gadh. Distributed optimal energy management in microgrids. *IEEE Transactions on Smart Grid*, 6(3):1137–1146, 2015.
47. Wenbo Shi, Na Li, Chi-Cheng Chu, and Rajit Gadh. Real-time energy management in microgrids. *IEEE Transactions on Smart Grid*, 2015.
48. Zhaoyu Wang, Bokan Chen, Jianhui Wang, Miroslav M Begovic, and Chen Chen. Coordinated energy management of networked microgrids in distribution systems. *IEEE Transactions on Smart Grid*, 6(1):45–53, 2015.
49. Nerea Ruiz, Iñigo Cobelo, and José Oyarzabal. A direct load control model for virtual power plant management. *IEEE Transactions on Power Systems*, 24(2):959–966, 2009.
50. Marco Giuntoli and Davide Poli. Optimized thermal and electrical scheduling of a large scale virtual power plant in the presence of energy storages. *IEEE Transactions on Smart Grid*, 4(2):942–955, 2013.

51. Elaheh Mashhour and Seyed Masoud Moghaddas-Tafreshi. Bidding strategy of virtual power plant for participating in energy and spinning reserve markets – part i: problem formulation. *IEEE Transactions on Power Systems*, 26(2):949–956, 2011.
52. E. Mashhour and S. M. Moghaddas-Tafreshi. Bidding strategy of virtual power plant for participating in energy and spinning reserve markets – part ii: numerical analysis. *IEEE Transactions on Power Systems*, 26(2):957–964, 2011.
53. Hongming Yang, Dexin Yi, Junhua Zhao, and Zhaoyang Dong. Distributed optimal dispatch of virtual power plant via limited communication. *IEEE Transactions on Power Systems*, 3(28):3511–3512, 2013.

Chapter 2
Optimal Energy Management for Smart Homes

2.1 System Model

Consider a smart home owning a mix of DERs such as renewable generators, storage devices, and energy loads. It may purchase power from the grid under the real-time pricing program. We assume a discrete-time model with time period indexed by t, where the length of each time period could be 15 min.

We first describe the mathematical models for renewable energy generation, energy storage, and electricity market we use in this chapter for the energy supply part as shown in Fig. 2.1. We then present the control objective, which is to minimize the long-term time-average expected electricity cost. In the next two sections, we consider two different types of energy demand, i.e., the inelastic energy demand and the elastic one, and further analyze the electricity cost minimization problem.

2.1.1 Renewable Energy Generation

Let $S(t)$ denote the amount of renewable energy generated in slot t and we assume that this energy is first stored in battery before it can be used in the next time slot. A controller is to regulate the portion $\gamma(t)$ of the generated energy stored into battery for each slot t in order to prevent battery overflow. The other portion is spilled. Hence, we have

$$0 \leq \gamma(t) \leq 1. \tag{2.1}$$

Moreover, there is a maximum value S_{max} for $S(t)$, that is,

$$0 \leq S(t) \leq S_{max}. \tag{2.2}$$

Y. Guo et al., *Stochastic Optimization for Distributed Energy Resources in Smart Grids*, SpringerBriefs in Electrical and Computer Engineering,
DOI 10.1007/978-3-319-59529-0_2

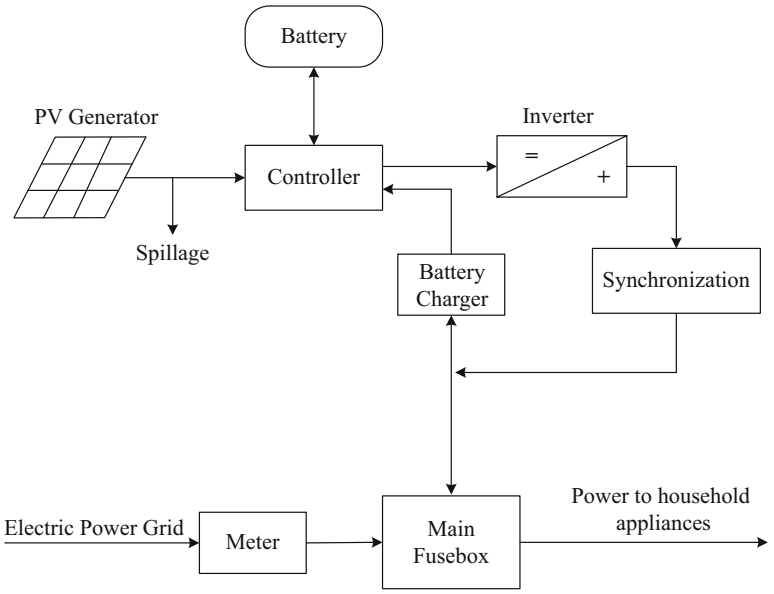

Fig. 2.1 A PV-utility grid system with battery storage for a smart home in smart grids

2.1.2 Energy Storage

In practice, the battery is not ideal and has the following physical properties as analyzed in [1, 2]. First, the battery lifetime depends on both the number of times it undergoes charging/discharging and the depth of discharge during its operation. This relationship is illustrated as battery lifetime chart [3]. Second, there is an energy conversion loss during the charging or discharging process, which is measured as charging/discharging efficiency. Finally, as the time goes, the battery will leak some energy stored in it. To simplify our analysis, we assume a battery model without any inefficiency in charging or discharging. As the time slot we choose is typically small (e.g., 5 min period), energy leakage over time can be neglected. However, more complicated battery model can be easily incorporated into our model without significant impact on our analysis.

We assume that in each time slot t, energy amount $G_b(t)$ can be drawn from the traditional power grid (or simply power grid) to recharge the battery in order to utilize the time-diversity of electricity price. The intuition is that if we recharge the battery when electricity price is low, the overall electricity cost may be reduced with proper design.

The state of charge (SOC) level $B(t)$ in the battery evolves according to the following equation:

$$B(t+1) = B(t) - D(t) + \gamma(t)S(t) + G_b(t), \tag{2.3}$$

where $D(t)$ is the amount of energy that is discharged from battery to supply demand in slot t. Obviously, we should have the following "energy-availability" and finite capacity constraint for each time slot t:

$$D(t) \leq B(t) \leq B_{max}, \tag{2.4}$$

where B_{max} is the battery capacity. There is a maximum discharge rate D_{max} of the battery for one time slot, i.e.,

$$0 \leq D(t) \leq D_{max}. \tag{2.5}$$

The energy amount that can be drawn from the electric power grid to recharge battery for one time slot is also bounded by G_b^{max}, i.e.,

$$0 \leq G_b(t) \leq G_b^{max}. \tag{2.6}$$

2.1.3 Electricity Market

As shown in [4], electricity price in the real-time electricity market has both time-diversity and location-diversity. In this paper, as the proof of concept, we concentrate on one single residential customer (one household), who is subject to a time-varying electricity price. Assume that the time-varying electricity price, $C(t)$, is sent to the customer's smart meter by the utility company at the beginning of each slot t. The cost of using renewable energy generated by the customer itself is assumed to be zero. Denote $G_l(t)$ as the power drawn from the electric power grid to directly supply the energy demand in slot t. Since the total electricity drawn from the electric power grid is $G_b(t) + G_l(t)$, the electricity cost for each time slot t is $(G_b(t) + G_l(t))C(t)$. In our analysis, the unit electricity price $C(t)$ does not depend on the total amount of energy drawn from the power grid. However, if the unit electricity price depends on the total power consumed, such as inclining block rate in [5], it can be still integrated easily into our model as in [1].

2.1.4 Control Objective

In this chapter, we are interested in long-term electricity cost. Hence, our objective here is to minimize the long-term time-average expected electricity cost as described below:

$$P = \lim_{T\to\infty} \frac{1}{T} \sum_{t=0}^{T-1} \mathbb{E}\{C(t)(G_l(t) + G_b(t))\}, \tag{2.7}$$

where the expectation is w.r.t. possibly randomized control actions as well as the distribution of electricity price $C(t)$.

2.2 Inelastic Energy Demand

In a smart home, some energy demands are inelastic, such as lighting, TV watching, as well as computers. For this kind of energy demands, the energy requests must be met exactly at the time t when needed. Based on the models presented in the previous section, we come up with a schematic of power management for inelastic energy demands depicted in Fig. 2.2, where both the power flow and the information flow are shown. Due to the information and communication infrastructure deployed in smart grids, a residential house would form a home area network, which enables communication between components for information gathering and dissemination.

We assume the inelastic energy demand generated in time slot t is $A_{ine}(t)$. For each time slot t, we have

$$G_l(t) + D(t) = A_{ine}(t). \tag{2.8}$$

Thus, our problem can be formulated as the following stochastic optimization, called **Problem One**:

$$\min_{D(t),G_b(t),G_l(t),\gamma(t)} P_1 = \lim_{T\to\infty} \frac{1}{T} \sum_{t=0}^{T-1} \mathbb{E}\{C(t)(G_l(t) + G_b(t))\} \tag{2.9}$$

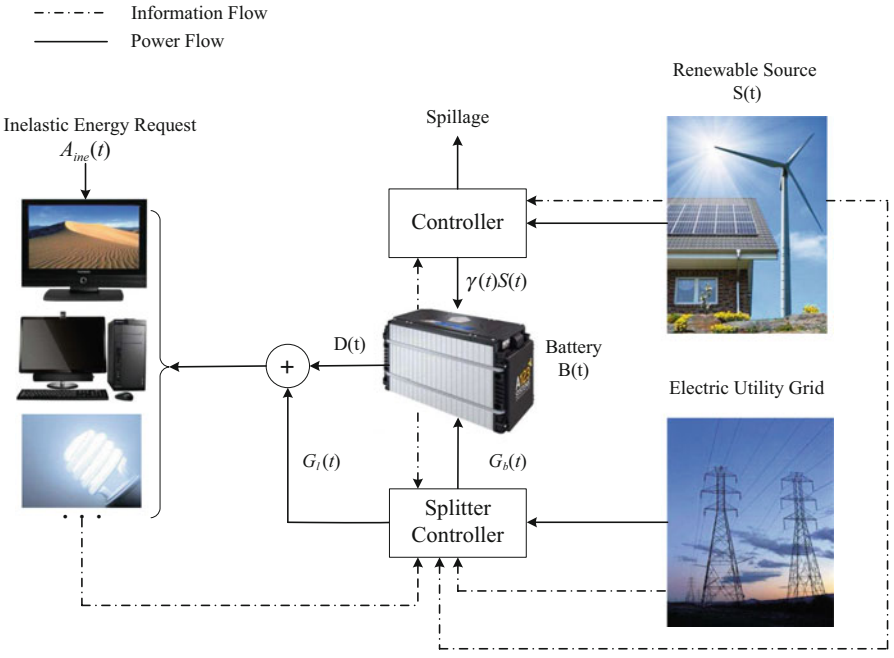

Fig. 2.2 A schematic of power management with inelastic energy demands in a smart home

subject to

$$B(t+1) = B(t) - D(t) + \gamma(t)S(t) + G_b(t),$$
$$D(t) \leq B(t) \leq B_{max},$$
$$G_l(t) + D(t) = A_{ine}(t),$$
$$0 \leq D(t) \leq D_{max},$$
$$0 \leq G_l(t) \leq G_l^{max}, 0 \leq G_b(t) \leq G_b^{max},$$
$$0 \leq \gamma(t) \leq 1.$$

Define the optimal objective value of the optimization problem above as P_1^*. In the following, we apply the Lyapunov optimization framework [6, 7] to find an approximate solution, which attains an analytical performance guarantee within $O(1/V)$ of the optimal objective value, where V is a tunable control parameter related to the battery capacity.

The problem above is challenging mainly because of the time-coupling property brought by the battery constraint (2.4). To be specific, in our problem, the current control action may impact the future control actions in the sense that a current action may overuse the battery and leave insufficient energy for future use, or the current action may leave less available capacity and the future generated renewable energy cannot be utilized efficiently. Previous methods to handle this time-coupling problem are usually based on dynamic programming, which suffers from the "curse of dimensionality" problem [8] and requires detailed knowledge of statistics of $C(t)$, $S(t)$ and $A_{ine}(t)$ in our problem. However, in reality, the statistics of $C(t)$, $S(t)$ and $A_{ine}(t)$ may be unknown or difficult to obtain, and we need to design an optimal control algorithm under uncertainty. We use the recently developed Lyapunov optimization framework [7] and find a modified Lyapunov function to develop our algorithm. A salient feature of our algorithm is that it does not need any future knowledge of the system states and can be implemented in real-time.

In the next subsection, instead of solving the above stochastic optimization problem exactly, we study a relaxed problem, whose solution is easy to characterize based on the framework of Lyapunov optimization [6, 7].

2.2.1 Relaxed Problem

We define the time-average expected value of utilized renewable energy, charging and discharging rate under any feasible control policy of **Problem One**, respectively, as follows.

$$\overline{\gamma S} = \lim_{T\to\infty} \frac{1}{T} \sum_{t=0}^{T-1} \mathbb{E}\{\gamma(t)S(t)\},$$

$$\overline{G_b} = \lim_{T\to\infty} \frac{1}{T} \sum_{t=0}^{T-1} \mathbb{E}\{G_b(t)\},$$

$$\overline{D} = \lim_{T\to\infty} \frac{1}{T} \sum_{t=0}^{T-1} \mathbb{E}\{D(t)\}.$$

Since the battery SOC level evolves according to (2.3), summing over all $t \in \{0, 1, 2, \ldots, T-1\}$ and taking expectation on both sides, we have

$$\mathbb{E}\{B(T)\} - B_0 = \sum_{t=0}^{T-1} \mathbb{E}\{\gamma(t)S(t) + G_b(t) - D(t)\},$$

where $B(0) = B_0$ is the initial battery SOC level. As $0 \le B(t) \le B_{max}$ for any time slot t, dividing both sides with T and taking $T \to \infty$, we have $\overline{D} = \overline{\gamma S} + \overline{G_b}$. Hence, we obtain the following relaxed problem, called **Problem Two**:

$$\min_{D(t),G_b(t),G_l(t),\gamma(t)} P_1 = \lim_{T\to\infty} \frac{1}{T} \sum_{t=0}^{T-1} \mathbb{E}\{C(t)(G_l(t) + G_b(t))\} \tag{2.10}$$

subject to

$$\overline{D} = \overline{\gamma S} + \overline{G_b},$$

$$G_l(t) + D(t) = A_{ine}(t),$$

$$0 \le D(t) \le D_{max},$$

$$0 \le G_l(t) \le G_l^{max}, 0 \le G_b(t) \le G_b^{max},$$

$$0 \le \gamma(t) \le 1.$$

Denote the optimal objective value of **Problem Two** as $P^*_{1,rel}$. From the discussion above, we observe that any feasible solution to **Problem One** is also a feasible solution to **Problem Two**, i.e., **Problem Two** is less constrained than **Problem One**. Therefore, $P^*_{1,rel} \le P^*_1$.

It is easy to find the optimal solution to **Problem Two** due to the removal of dependence between battery SOC levels across time slots. As given by the following lemma, the optimal solution to **Problem Two** can be obtained by a randomized, stationary control policy that only chooses $D(t)$, $G_l(t)$, $G_b(t)$ and $\gamma(t)$ every slot purely as a (possibly randomized) function of $C(t)$, $S(t)$ and $A_{ine}(t)$. That means the control policy is independent of battery SOC level. This fact is stated as below:

Lemma 2.1 *If the* $\{A_{ine}(t), C(t), S(t)\}$ *are i.i.d. over slots, then there exists a stationary and randomized policy that takes control decisions* $\hat{D}_{ine}(t)$, $\hat{G}_{l,ine}(t)$, $\hat{G}_{b,ine}(t)$ *and* $\hat{\gamma}_{ine}(t)$ *every slot t purely as a function (possibly randomized) of current system states* $\{A_{ine}(t), C(t), S(t)\}$ *while satisfying the constraints above and providing the following guarantees:*

$$\mathbb{E}\{\hat{D}_{ine}(t)\} = \mathbb{E}\{\hat{\gamma}_{ine}S(t)\} + \mathbb{E}\{\hat{G}_{b,ine}(t)\}, \tag{2.11}$$

$$\mathbb{E}\{C(t)(\hat{G}_{l,ine}(t) + \hat{G}_{b,ine}(t))\} = P^*_{1,rel}, \tag{2.12}$$

where the expectations are w.r.t. the stationary distribution of $\{A_{ine}(t), C(t), S(t)\}$ *and randomized control decisions.*

The proof is similar to that in [1, 9] and follows directly from the framework of Lyapunov optimization in [6, 7], which is omitted here for brevity.

To derive such a policy, we need to know the statistical distribution of all combinations of $\{A_{ine}(t), C(t), S(t)\}$, which suffers from the "curse of dimensionality" problem [8] if being solved by dynamic programming. Moreover, this control policy may not be a feasible solution to **Problem One**. Instead, we use the existence of such a policy to help us design our control policy that meets all constraints of **Problem One** and derive the performance results for our algorithm.

2.2.2 Our Proposed Algorithm

Before presenting our algorithm, we define another variable $X_{ine}(t)$ as a shifted version of battery SOC level $B(t)$ for each time slot t as follows:

$$X_{ine}(t) = B(t) - V_{ine}C_{max} - D_{max}, \tag{2.13}$$

where V_{ine} is a control parameter to be specified later. $X_{ine}(t)$ is used to ensure that the constraint (2.4) of battery SOC level is satisfied in our algorithm. The intuition behind $X_{ine}(t)$ is to construct the algorithm based on a quadratic Lyapunov function, but carefully perturb the weights used for decision making, so as to push the SOC level in battery towards certain nonzero values to avoid underflow. According to (2.3) of $B(t)$, we have the same update equation for $X_{ine}(t)$,

$$X_{ine}(t+1) = X_{ine}(t) - D(t) + \gamma(t)S(t) + G_b(t). \tag{2.14}$$

In the latter part of this paper, we will prove that through our algorithm, $X_{ine}(t)$ is bounded in some range so that the constraint (2.4) on $B(t)$ is always satisfied for each slot t.

The proposed algorithm for inelastic energy demand is shown in Algorithm 1. Note that the algorithm only uses the current system states $X_{ine}(t)$, $C(t)$, $S(t)$ and $A_{ine}(t)$, and does not require any knowledge of the statistics of renewable energy generation, electricity price, and energy demand arrival process.

foreach *Time slot t* **do**

1 Measure the system states $X_{ine}(t)$, $C(t)$, $S(t)$ and $A_{ine}(t)$;

2 Choose control decisions $D^*_{ine}(t)$, $G^*_{l,ine}(t)$, $G^*_{b,ine}(t)$ and $\gamma^*_{ine}(t)$ as the solution to the following optimization problem, called **Problem Three**:

$$\begin{aligned}
&\min \ [V_{ine}C(t) + X(t)]G_b(t) + [X(t)S(t)]\gamma(t) + [V_{ine}C(t)]G_l(t) - X(t)D(t) \\
&\text{s.t.} \\
&\qquad D(t) + G_l(t) = A_{ine}(t), \\
&\qquad 0 \le G_l(t) \le G_l^{max}, 0 \le G_b(t) \le G_b^{max}, \\
&\qquad 0 \le D(t) \le D_{max}, \\
&\qquad 0 \le \gamma(t) \le 1;
\end{aligned}$$

3 $X(t+1) = X(t) - D^*_{ine}(t) + \gamma^*_{ine}(t)S(t) + G^*_{b,ine}(t)$;

end

Algorithm 1: Power management with inelastic energy demands

2.2.3 Algorithmic Properties

In this subsection, we summarize the properties of our proposed algorithm as follows.

Theorem 2.1 *Assume that* $G_l^{max} + G_b^{max} \ge A_{ine}^{max}$, *then for any parameter* V_{ine} *satisfying* $0 < V_{ine} \le V_{ine}^{max}$ *for all* $t \in \{0, 1, 2, \ldots\}$, *where*

$$V_{ine}^{max} \triangleq \frac{B_{max} - D_{max} - G_b^{max} - S_{max}}{C_{max} - C_{min}}, \tag{2.15}$$

our Algorithm 3 has the following properties:

1. *The queue* $X(t)$ *is always lower and upper bounded for all slots t as follows*

$$X(t) \ge -V_{ine}C_{max} - D_{max},$$

and

$$X(t) \leq B_{max} - V_{ine}C_{max} - D_{max}.$$

2. *All control decisions are feasible.*
3. *If $S(t)$, $C(t)$ and $A_{ine}(t)$ are i.i.d. over slots, then the time-average expected cost under our algorithm is within bound B_1/V_{ine} of the optimal value, i.e.,*

$$\lim_{T\to\infty} \frac{1}{T} \sum_{t=0}^{T-1} \mathbb{E}\{C(t)(G_l(t) + G_b(t))\} \leq P_1^* + B_1/V_{ine}, \tag{2.16}$$

where B_1 is a constant given by

$$B_1 \triangleq \frac{[(G_b^{max} + S_{max})^2, D_{max}^2]}{2}. \tag{2.17}$$

Proof See Appendix 2.4.2.

2.3 Elastic Energy Demand

While the previous section deals with inelastic energy demand, some household appliances in the smart home can be made "smart", meaning that they can be controlled to adjust the times of their operations and the amount of their energy usage. In other words, as long as their energy requirements are met within certain deadlines, the residential customers will be satisfied. Some typical examples include dish washer, water heater, air conditioning, and charging of PHEVs. A schematic for the power management with elastic energy demands is shown in Fig. 2.3.

We assume that the amount of elastic energy demands requested at slot t is $A_{ela}(t)$. These energy demands are stored in an energy demand queue. In every slot t, the energy discharged from the battery is denoted as $D(t)$ and the energy amount drawn directly from the power grid is denoted as $G_l(t)$, which are determined from the buffered energy demands. The energy demands are served in a First-In-First-Out (FIFO) manner.

Let $Q(t)$ denote the total energy demands in the queue for time slot t, we have the following queuing equation:

$$Q(t+1) = max\{Q(t) - D(t) - G_l(t), 0\} + A_{ela}(t). \tag{2.18}$$

As long as the waiting time of any buffered energy demand in this demand queue does not exceed a certain maximum deadline δ_{max}, the utility perceived by customers does not decrease. We use the same battery model (2.3) as in the case for inelastic energy demands. Our problem here is to minimize the time-average expected

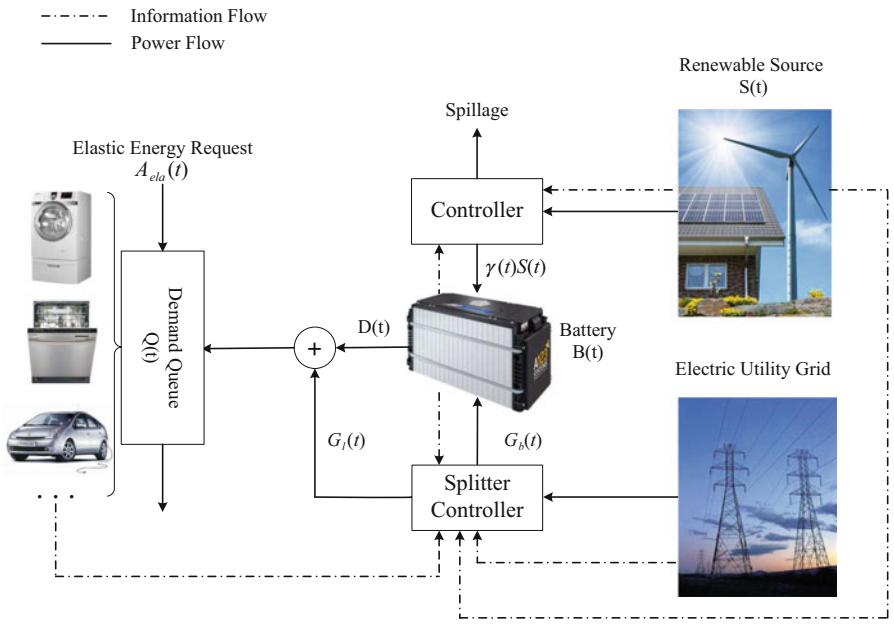

Fig. 2.3 A schematic for power management with elastic energy demands in the smart grid

electricity cost subject to all constraints discussed before and to ensure finite average delay for any buffered energy demand, which can be stated below and is called **Problem Four**:

$$\min_{D(t),G_b(t),G_l(t),\gamma(t)} P_2 = \lim_{T\to\infty} \frac{1}{T} \sum_{t=0}^{T-1} \mathbb{E}\{C(t)(G_l(t) + G_b(t))\} \tag{2.19}$$

subject to

$$\begin{aligned} B(t+1) &= B(t) - D(t) + \gamma(t)S(t) + G_b(t), \\ D(t) &\le B(t) \le B_{max}, \\ Q(t+1) &= max\{Q(t) - D(t) - G_l(t), 0\} + A_{ela}(t), \\ 0 &\le D(t) \le D_{max}, \\ 0 &\le G_b(t) \le G_b^{max}, 0 \le G_l(t) \le G_l^{max}, \\ 0 &\le \gamma(t) \le 1, \\ \overline{Q} &< \infty, \end{aligned} \tag{2.20}$$

where $\overline{Q}$ is the time-average expected energy demand queue backlog defined as:

$$\overline{Q} = \lim_{T\to\infty} \frac{1}{T} \sum_{t=0}^{T-1} \mathbb{E}\{Q(t)\}.$$

2.3.1 Relaxed Problem

Similar to the case for the inelastic energy demands, we define a relaxed problem, called **Problem Five**, which can be stated as follows:

$$\min_{D(t),G_b(t),G_l(t),\gamma(t)} P_2 = \lim_{T\to\infty} \frac{1}{T} \sum_{t=0}^{T-1} \mathbb{E}\{C(t)(G_l(t) + G_b(t))\} \tag{2.21}$$

subject to

$$\overline{D} = \overline{\gamma S} + \overline{G_b},$$
$$Q(t+1) = max\{Q(t) - D(t) - G_l(t), 0\} + A_{ela}(t),$$
$$0 \le D(t) \le D_{max},$$
$$0 \le G_b(t) \le G_b^{max}, 0 \le G_l(t) \le G_l^{max},$$
$$0 \le \gamma(t) \le 1,$$
$$\overline{Q} < \infty.$$

Denote the optimal objective value of **Problem Four** and **Problem Five** as P_2^* and $P_{2,rel}^*$, respectively. Similarly, any feasible solution to **Problem Four** is also a feasible solution to **Problem Five**, therefore, $P_{2,rel}^* \le P_2^*$. Similar to Lemma 2.1, we have the following result:

Lemma 2.2 *If $\{A_{ela}(t), C(t), S(t)\}$ are i.i.d. over slots, then there exists a stationary and randomized policy that takes control decisions $\hat{D}_{ela}(t)$, $\hat{G}_{l,ela}(t)$, $\hat{G}_{b,ela}(t)$ and $\hat{\gamma}_{ela}(t)$ every slot t purely as a (possibly randomized) function of current system states $\{A_{ela}(t), C(t), S(t)\}$ while satisfying the constraints above and providing the following guarantees:*

$$\mathbb{E}\{\hat{D}_{ela}(t)\} = \mathbb{E}\{\hat{\gamma}_{ela}S(t)\} + \mathbb{E}\{\hat{G}_{b,ela}(t)\}, \tag{2.22}$$
$$\mathbb{E}\{\hat{D}_{ela}(t) + \hat{G}_{l,ela}(t)\} \ge \mathbb{E}\{A_{ela}(t)\}, \tag{2.23}$$
$$\mathbb{E}\{C(t)(\hat{G}_{l,ela}(t) + \hat{G}_{b,ela}(t))\} = P_{2,rel}^*, \tag{2.24}$$

where the expectations are w.r.t. the stationary distribution of $\{A_{ela}(t), C(t), S(t)\}$ *and the randomized control decisions.*

The proof is similar to that in [1, 9] and follows directly from the framework of Lyapunov optimization in [6, 7], which is omitted here for brevity.

Note that the constraint (2.20) only ensures finite average delay without any guarantee for the worst-case delay. In the following, we use the technique of ε-persistent queue [10] to guarantee the finite worst-case delay for any buffered energy demand in the queue.

2.3.2 Delay-Aware Virtual Queue

We use the following virtual queue $Z(t)$ to provide the worst-case delay guarantee on any buffered energy demand in $Q(t)$:

$$Z(t+1) = \max\{Z(t) - D(t) - G_l(t) + \varepsilon 1_{\{Q(t)>0\}}, 0\}, \tag{2.25}$$

where $1_{\{Q(t)>0\}}$ is an indicator function that is 1 if $Q(t) > 0$ or 0 otherwise, and ε is a fixed positive parameter to be specified later. The intuition behind this virtual queue is that since $Z(t)$ has the same service process as $Q(t)$, but has an arrival process that adds ε whenever the actual backlog is nonempty, this ensures that $Z(t)$ grows if there is energy demand in the queue $Q(t)$ that has not been serviced for a long time. The following lemma shows that if we can control the system to ensure that the queues $Q(t)$ and $Z(t)$ have finite upper bounds, then any buffered energy demand is served within the worst-case delay.

Lemma 2.3 *Suppose we can control the system to ensure that* $Z(t) \leq Z_{max}$ *and* $Q(t) \leq Q_{max}$ *for all slots t, where* Z_{max} *and* Q_{max} *are some positive constants, then the worst-case delay for all buffered energy demand is upper bounded by* δ_{max} *slots where*

$$\delta_{max} \triangleq \lceil \frac{(Q_{max} + Z_{max})}{\varepsilon} \rceil. \tag{2.26}$$

Proof The proof follows directly from the framework of Lyapunov optimization [7] and is given in Appendix 3.5.2 for completeness.
We will show that there indeed exist such constants Z_{max} and Q_{max} later.

2.3.3 Our Proposed Algorithm

Before presenting our algorithm, we define another variable $X_{ela}(t)$ as a shifted version of battery SOC level $B(t)$ for time slot t as follows:

$$X_{ela}(t) = B(t) - \Theta_{max} - D_{max}, \tag{2.27}$$

where Θ_{max} is a positive constant to be specified. $X_{ela}(t)$ is also used to ensure that the constraint (2.4) of battery SOC level is satisfied in our algorithm. According to Eq. (2.3), we obtain the same update equation for $X_{ela}(t)$,

$$X_{ela}(t+1) = X_{ela}(t) - D(t) + \gamma(t)S(t) + G_b(t). \tag{2.28}$$

The algorithm for elastic energy demands is shown in Algorithm 4. Similarly, the algorithm only makes use of the current system states $(X_{ela}(t), Q(t), Z(t))$, $C(t)$, $S(t)$ and $A_{ela}(t)$, and does not require any knowledge on the statistics of the renewable energy generation, the electricity price, and the energy demand arrival process.

foreach *Time slot t* **do**

1 Measure system states $(X_{ela}(t), Q(t), Z(t))$, $C(t)$, $S(t)$ and $A_{ela}(t)$;

2 Choose control decisions $D^*_{ela}(t)$, $G^*_{l,ela}(t)$, $G^*_{b,ela}(t)$ and $\gamma^*_{ela}(t)$ as the solution to the following optimization problem, called **Problem Six**:

$$\min \ [V_{ela}C(t) + X_{ela}(t)]G_b(t) + [X_{ela}(t)S(t)]\gamma(t) + [V_{ela}C(t) - Z(t) - Q(t)]G_l(t) - [X_{ela}(t) + Z(t) + Q(t)]D(t)$$

s.t.

$$0 \le D(t) \le D_{max},$$

$$0 \le G_l(t) \le G_l^{max}, 0 \le G_b(t) \le G_b^{max},$$

$$0 \le \gamma(t) \le 1;$$

3 $X(t+1) = X(t) - D^*_{ela}(t) + \gamma^*_{ela}(t)S(t) + G^*_{b,ela}(t)$;

4 $Z(t+1) = \max[Z(t) - D^*_{ela}(t) - G^*_{l,ela}(t) + \varepsilon 1_{\{Q(t)>0\}}, 0]$;

5 $Q(t+1) = \max[Q(t) - D^*_{ela}(t) - G^*_{l,ela}(t), 0] + A_{ela}(t)$;

end

Algorithm 2: Power management with elastic energy demands

2.3.4 Algorithmic Properties

In this subsection, we summarize the properties of our proposed algorithm as follows.

Theorem 2.2 *Assume that* $G_l^{max} \ge \max[A_{ela}^{max}, \varepsilon]$. *If* $Q(0) = Z(0) = 0$, *then for any fixed parameter* $0 \le \varepsilon \le \mathbb{E}\{A(t)\}$ *and a parameter* V_{ela} *such that* $0 < V_{ela} \le V_{ela}^{max}$ *for all* $t \in \{0, 1, 2, \ldots\}$, *where*

$$V_{ela}^{max} \triangleq \frac{B_{max} - A_{ela}^{max} - \varepsilon - D_{max} - G_b^{max} - S_{max}}{C_{max} - C_{min}}, \tag{2.29}$$

our Algorithm 4 has the following properties:

1. *The queues $Q(t)$ and $Z(t)$ are deterministically upper bounded by Q_{max} and Z_{max} at every slot, where:*

$$Q_{max} \triangleq V_{ela}C_{max} + A_{ela}^{max}, \quad Z_{max} \triangleq V_{ela}C_{max} + \varepsilon. \tag{2.30}$$

Further, $Q(t) + Z(t)$ are upper bounded by Θ_{max} where

$$\Theta_{max} \triangleq V_{ela}C_{max} + A_{ela}^{max} + \varepsilon. \tag{2.31}$$

2. *The worst-case delay of any buffered energy demand is given by:*

$$\delta_{max} = \lceil \frac{2V_{ela}C_{max} + A_{ela}^{max} + \varepsilon}{\varepsilon} \rceil. \tag{2.32}$$

3. *The queue $X_{ela}(t)$ is always lower and upper bounded for all slots t by the following:*

$$-\Theta_{max} - D_{max} \leq X_{ela}(t) \leq B_{max} - \Theta_{max} - D_{max}.$$

4. *All control decisions are feasible.*
5. *If $S(t)$, $C(t)$, and $A_{ela}(t)$ are i.i.d. over slots, then the time-average expected electricity cost under our algorithm is within bound B_2/V_{ela} of the optimal value, i.e.,*

$$\lim_{T\to\infty} \frac{1}{T} \sum_{t=0}^{T-1} \mathbb{E}\{C(t)(G_l(t) + G_b(t))\} \leq P_2^* + B_2/V_{ela}, \tag{2.33}$$

where B_2 is a constant given by

$$\begin{aligned} B_2 \triangleq & \frac{[(D_{max} + G_l^{max})^2 + A_{ela,max}^2]}{2} \\ & + \frac{\max[(D_{max} + G_l^{max})^2, \varepsilon^2]}{2} \\ & + \frac{\max[(S_{max} + G_b^{max})^2, D_{max}^2]}{2}. \end{aligned} \tag{2.34}$$

Proof See Appendix 2.4.2.

2.4 Performance Evaluation

In this section, we evaluate the proposed algorithms using practical data sets of electricity price and renewable energy generation. We consider a single household with a battery, a PV panel and various appliances subject to real-time pricing.

2.4.1 Simulation Setup

The data set of electricity price we use is from the California Independent System Operator (CAISO) [11] for Los Angeles area, which consists of 5 min interval average spot market price $C(t)$. Meanwhile, we use the 5 min interval average solar irradiance data for Los Angels area from the Measurement and Instrumentation Data center (MIDC) [12] at National Renewable Energy Laboratory. The period we consider in this paper is half year from January 1, 2011 to June 30, 2011. In total, this duration includes 181 days or 52, 128 5 min slots. The control interval is chosen to be 5 min. A portion of average hourly spot market electricity price and solar irradiance during the first week of January 2011 are plotted in Figs. 2.4 and 2.5, respectively.

We execute our algorithms in 5 min time slots and experiment with different values of parameters V, B_{max}, and ε. In our simulation, we set the energy demand arrival, either elastic or inelastic, during each time slot t as uniformly distributed from [1, 24] KW-slot based on the practical home appliance usage in [5]. We fix the parameters $D_{max} = 30$ KW-slot, $G_l^{max} = 30$ KW-slot, and $G_b^{max} = 20$ KW-slot.

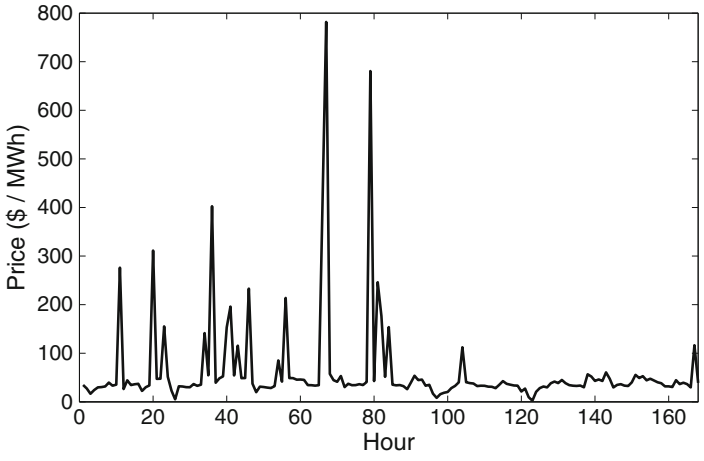

Fig. 2.4 Average hourly spot market price during the week of 01/01/2011 to 01/07/2011 at LA [11]

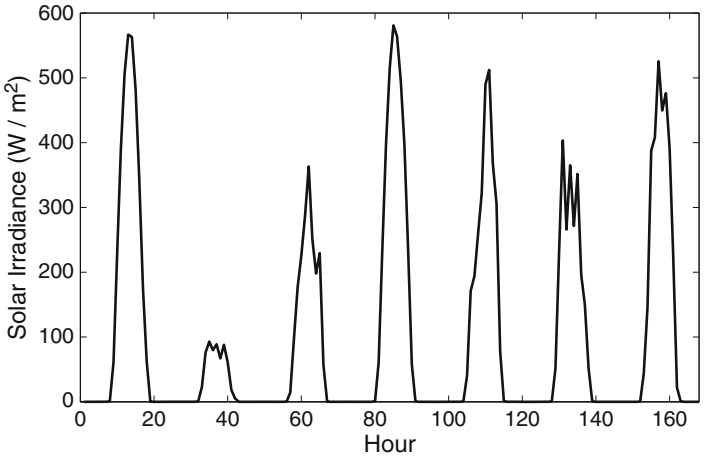

Fig. 2.5 Average hourly solar irradiance profile during the week of 01/01/2011 to 01/07/2011 at LA [12]

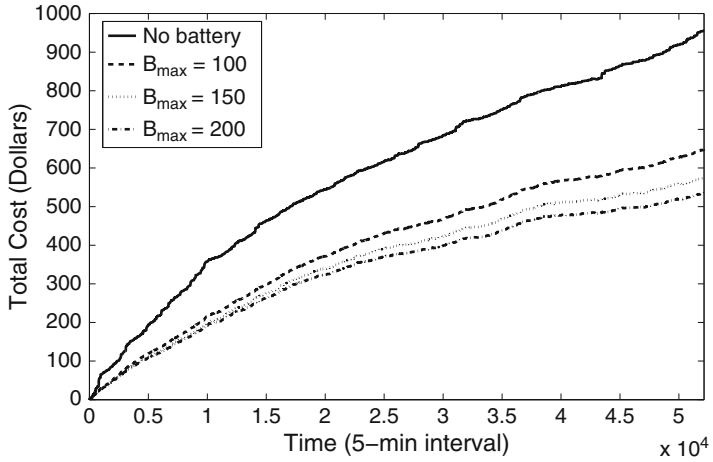

Fig. 2.6 Total Cost with i.i.d. A(t) and different battery capacity B_{max} for inelastic energy demands

2.4.2 Results and Analysis

First, we consider the impact of storage capacity B_{max} on cost saving in the case for inelastic energy demands. We compare our algorithm against a simple algorithm without storage. The simple algorithm uses the renewable energy generation to meet the demand as much as possible; in the case of insufficiency, it would draw some power from the power grid to meet the energy demand. The result is illustrated in Fig. 2.6 during 6-month period with $B_{max} = \{100, 150, 200\}$ KW-slot and

$V = V_{ine}^{max}$. From the figure, it is clear that the larger the battery is, the more saving our proposed algorithm can obtain. The saving comes from two aspects: one is by storing excessive renewable energy generated in current time slot for use at later time when renewable energy generation is insufficient; the other is by charging the battery when price is low while discharging it when price is high.

Next, we compare the cases for the inelastic energy demand and the elastic one when $B_{max} = 100$ KW-slot, $\varepsilon = 1$, and $V = V_{ine}^{max}$. The result is shown in Fig. 2.7. The case when the battery is used in conjunction with elastic energy demand provides more spaces to optimize the cost saving, as illustrated in the figure. This result is intuitive as some elastic energy demands can be delayed to time when free renewable energy is sufficient or the electricity price is low.

Finally, we consider the impact of ε on the performance of our algorithm for the case for elastic energy demands. As explained before, ε is related to the worst-case delay of queued energy demands. Smaller ε implies larger delay. We set $B_{max} = 100$ KW-slot and $V = V_{ela}^{max}$, and select different $\varepsilon \in \{0, 0.3, 0.6, 1\}$. As observed in Fig. 2.8, the decrease in ε gives lower cost with the tradeoff that the worst-case delay is increased.

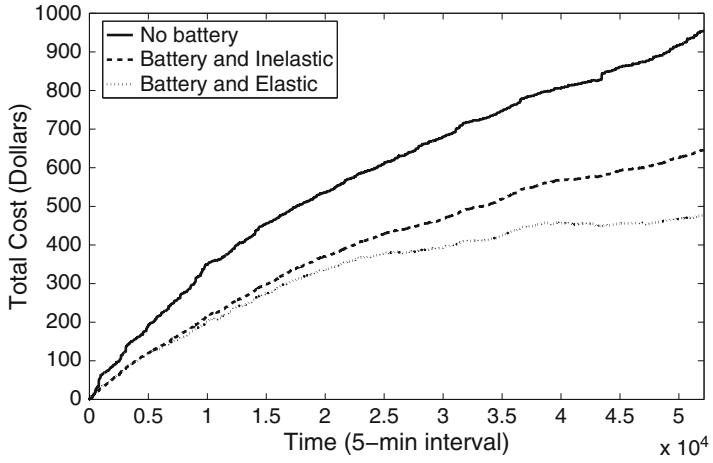

Fig. 2.7 Comparison of total cost for the cases when there is no battery, there is battery with inelastic energy demands, and there is battery with elastic energy demands

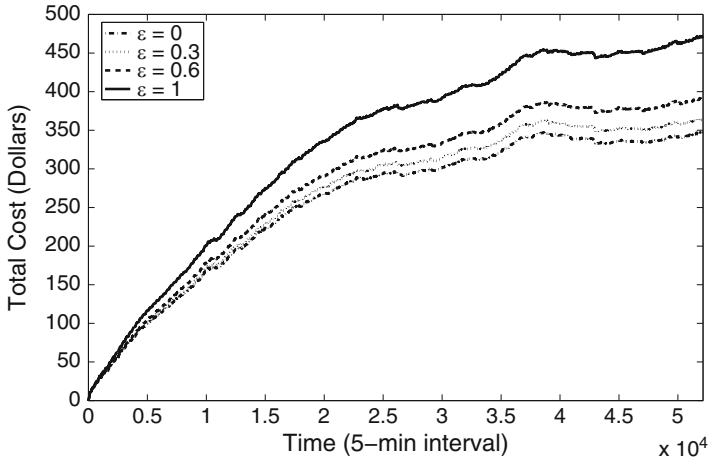

Fig. 2.8 Comparison of total cost for different ε with elastic energy demands

Appendix

Proof of Theorem 2.1

Here we prove Theorem 2.1.

Proof 1). It is obvious that the optimal solution to **Problem Three** has the following properties:

- If $X_{ine}(t) > -V_{ine}C_{min}$, $G^*_{b,ine}(t) = 0$ and $D^*_{ine}(t) = \min\{A_{ine}(t), D_{max}\}$.
- If $X_{ine}(t) < -V_{ine}C_{max}$, $G^*_{b,ine}(t) = G^{max}_b$ and $D^*_{ine}(t) = \max\{0, A_{ine}(t) - G^{max}_l\}$.

We now use induction to prove this result. When $t = 0$, as $X_{ine}(0) = B_0 - V_{ine}C_{max} - D_{max}$ and $0 \le B_0 \le B_{max}$, we have $-V_{ine}C_{max} - D_{max} \le X_{ine}(0) \le B_{max} - V_{ine}C_{max} - D_{max}$.

Now suppose that the above bound holds for time slot t. We need to prove that it also holds for time slot $t+1$. First, suppose $-V_{ine}C_{max} - D_{max} \le X_{ine}(t) < -V_{ine}C_{max}$, then $X_{ine}(t+1) = X_{ine}(t) + G^*_{b,ine}(t) + S(t) - D^*_{ine}(t) \ge -V_{ine}C_{max} - D_{max} + G^{max}_b - \max\{0, A_{ine}(t) - G^{max}_l\}$. As $G^{max}_l + G^{max}_b \ge A^{max}_{ine}$, we have $X_{ine}(t+1) \ge X_{ine}(t) \ge -V_{ine}C_{max} - D_{max}$. Moreover, $X_{ine}(t+1) \le X_{ine}(t) + G^{max}_b + S_{max} \le -V_{ine}C_{min} + G^{max}_b + S_{max} \le B_{max} - V_{ine}C_{max} - D_{max}$, where we have used

$$V_{ine} \le \frac{B_{max} - D_{max} - G^{max}_b - S_{max}}{C_{max} - C_{min}}.$$

Second, suppose $-V_{ine}C_{max} \leq X_{ine}(t) \leq -V_{ine}C_{min}$, then $-V_{ine}C_{max} - D_{max} \leq X_{ine}(t) - D_{max} \leq X_{ine}(t+1) \leq X_{ine}(t) + G_b^{max} + S_{max} \leq -V_{ine}C_{min} + G_b^{max} + S_{max} \leq B_{max} - V_{ine}C_{max} - D_{max}$, where we have used the same bound of V_{ine} as the case above. Third, suppose $-V_{ine}C_{min} < X_{ine}(t) \leq 0$, then $G_{b,ine}^*(t) = 0$. It is obvious that $X_{ine}(t+1) \geq X_{ine}(t) - D_{max} > -V_{ine}C_{max} - D_{max}$. Moreover, $X_{ine}(t+1) \leq X_{ine}(t) + S_{max} \leq S_{max} \leq B_{max} - V_{ine}C_{max} - D_{max}$, where we have used the upper bound of V_{ine} and $G_b^{max} \geq V_{ine}^{max}C_{min}$. Finally, suppose $0 < X_{ine}(t) \leq B_{max} - V_{ine}C_{max} - D_{max}$, then $G_{b,ine}^*(t) = \gamma_{ine}^*(t) = 0$. Hence $-V_{ine}C_{max} - D_{max} \leq X_{ine}(t+1) \leq X_{ine}(t) \leq B_{max} - V_{ine}C_{max} - D_{max}$. From the induction, we conclude the proof of 1).

2). From 1) and the definition (2.13) of $X_{ine}(t)$, it follows immediately that $0 \leq B(t) \leq B_{max}$ holds for any time slot t. Further, we make our decisions to satisfy all constraints in **Problem Three**. Combining them together, all constraints of **Problem One** are satisfied. Therefore, our control decisions are feasible to **Problem One**.

3). We make use of the Lyapunov optimization techniques [7] to derive the performance bound for our algorithm. Define the Lyapunov function as $L(X_{ine}(t)) = \frac{1}{2}X_{ine}^2(t)$ and the conditional 1-slot Lyapunov drift as follows:

$$\triangle(X_{ine}(t)) = \mathbb{E}\{L(X_{ine}(t+1)) - L(X_{ine}(t))|X_{ine}(t)\}.$$

From Eq. (2.14), squaring both sides, we obtain

$$\frac{X_{ine}^2(t+1) - X_{ine}^2(t)}{2} = \frac{(D(t) - \gamma(t)S(t) - G_b(t))^2}{2} - X_{ine}(t)(D(t) - \gamma(t)S(t) - G_b(t)).$$

As $0 \leq D(t) \leq D_{max}$ and $0 \leq \gamma(t)S(t) + G_b(t) \leq G_b^{max} + S_{max}$, we have

$$\frac{(D(t) - \gamma(t)S(t) - G_b(t))^2}{2} \leq \frac{1}{2}\max[(G_b^{max} + S_{max})^2, D_{max}^2].$$

Therefore, we can obtain the following upper bound on the Lyapunov drift for $X_{ine}(t)$:

$$\frac{X_{ine}^2(t+1) - X_{ine}^2(t)}{2} \leq \frac{1}{2}\max[(G_b^{max} + S_{max})^2, D_{max}^2] - X_{ine}(t)(D(t) - \gamma(t)S(t) - G_b(t)) \quad .$$

Taking expectation w.r.t. $X_{ine}(t)$ and adding the penalty term $V_{ine}\mathbb{E}\{C(t)(G_l(t) + G_b(t))|X_{ine}(t)\}$ to both sides of the inequality above, we obtain the following inequality:

$$\triangle(X_{ine}(t)) + V_{ine}\mathbb{E}\{C(t)(G_l(t) + G_b(t))|X_{ine}(t)\} \leq B_1$$

$$
\begin{aligned}
&- X_{ine}(t)\mathbb{E}\{D(t) - \gamma(t)S(t) - G_b(t)|X_{ine}(t)\} \\
&+ V_{ine}\mathbb{E}\{C(t)(G_l(t) + G_b(t))|X_{ine}(t)\},
\end{aligned}
$$

where B_1 is defined as

$$
B_1 \triangleq \frac{[(G_b^{max} + S_{max})^2, D_{max}^2]}{2}.
$$

Comparing with the objective of **Problem Three**, it is obvious that our algorithm always attempts to greedily minimize the right hand side (R.H.S.) of the inequality above for each time slot t over all possible feasible control policies including the optimal, stationary policy given in Lemma 2.1. Plugging this policy $(\hat{D}_{ine}(t), \hat{G}_{l,ine}(t), \hat{G}_{b,ine}(t), \hat{\gamma}_{ine}(t))$ into the R.H.S. of the inequality above and using the fact that this policy is independent of queue state $X_{ine}(t)$, we obtain the following:

$$
\begin{aligned}
\triangle(X_{ine}(t)) + V_{ine}\mathbb{E}\{C(t)(G_l(t) + G_b(t))|X_{ine}(t)\} &\leq B_1 \\
&- X_{ine}(t)\mathbb{E}\{\hat{D}_{ine}(t) - \hat{\gamma}_{ine}(t)S(t) - \hat{G}_{b,ine}(t)|X_{ine}(t)\} \\
&+ V_{ine}\mathbb{E}\{C(t)(\hat{G}_{l,ine}(t) + \hat{G}_{b,ine}(t))|X_{ine}(t)\} \\
&\leq B_1 + V_{ine}P_{1,rel}^* \leq B_1 + V_{ine}P_1^*,
\end{aligned}
$$

where the following facts have been used:

$$
\begin{aligned}
\mathbb{E}\{\hat{D}_{ine}(t) - \hat{\gamma}_{ine}(t)S(t) - \hat{G}_{b,ine}(t)|X_{ine}(t)\} &= 0, \\
\mathbb{E}\{C(t)(\hat{G}_{l,ine}(t) + \hat{G}_{b,ine}(t))|X_{ine}(t)\} &= P_{1,rel}^*.
\end{aligned}
$$

The equations above follow from Lemma 2.1. Taking the expectation on both sides, using the law of iterative expectation, and summing over $t \in \{0, 1, 2, \ldots, T-1\}$, we obtain

$$
\begin{aligned}
V_{ine}\sum_{t=0}^{T-1}\mathbb{E}\{C(t)(G_l(t) + G_b(t)) &\leq B_1 T + V_{ine}TP_1^* \\
&- \mathbb{E}\{L(X_{ine}(T))\} + \mathbb{E}\{L(X_{ine}(0))\}.
\end{aligned}
$$

Dividing both sides by T, letting $T \to \infty$, and using the facts that $E\{L(X_{ine}(0))\}$ are finite and $E\{L(X_{ine}(t))\}$ are nonnegative, we finally arrive at the following:

$$
\lim_{T\to\infty}\frac{1}{T}\sum_{t=0}^{T-1}\mathbb{E}\{C(t)(G_l(t) + G_b(t))\} \leq P_1^* + B_1/V_{ine},
$$

where P_1^* is the optimal objective value, B_1 is a constant given by Eq. (2.17), and V_{ine} is a control parameter which has a maximum value given by Eq. (2.15). This completes the proof of 3).

Proof of Lemma 3.1

Here we prove Theorem 3.1.

Proof Consider any slot t for which $A_{ela}(t) > 0$. We will show that this energy request $A_{ela}(t)$ is served on or before time $t + \delta_{max}$ by contradiction. Suppose not, then during slots $\tau \in \{t+1, \ldots, t+\delta_{max}\}$ it must be that $Q(\tau) > 0$, otherwise, the energy request $A_{ela}(t)$ would have been served before τ. Therefore, $1_{Q(t)>0} = 1$, and from the update Eq. (3.25) of $Z(t)$, we have for all $\tau = \{t+1, \ldots, t+\delta_{max}\}$:

$$Z(\tau+1) \geq Z(\tau) - D(t) - G_l(t) + \varepsilon.$$

Summing the above over $\tau = \{t+1, \ldots, t+\delta_{max}\}$ yields:

$$Z(t+\delta_{max}+1) - Z(t+1) \geq -\sum_{\tau=t+1}^{t+\delta_{max}} [D(t) + G_l(t)] + \delta_{max}\varepsilon.$$

Rearranging the terms and using the facts that $Z(t+1) \geq 0$ and $Z(t+\delta_{max}+1) \leq Z_{max}$ yields:

$$\sum_{\tau=t+1}^{t+\delta_{max}} [D(t) + G_l(t)] \geq \delta_{max}\varepsilon - Z_{max}. \tag{2.35}$$

Since the request $A_{ela}(t)$ are queued in a FIFO manner and $Q(t+1) \leq Q_{max}$, it would be served on or before time $t + \delta_{max}$ whenever there are at leat Q_{max} units of energy served during $\tau \in \{t+1, \ldots, t+\delta_{max}\}$. As we have assumed that the request $A_{ela}(t)$ are not served by time $t+\delta_{max}$, it must be that $\sum_{\tau=t+1}^{t+\delta_{max}} [D(t)+G_l(t)] < Q_{max}$. Comparing this inequality with (3.41) yields:

$$Q_{max} > \delta_{max}\varepsilon - Z_{max},$$

which implies that $\delta_{max} < (Q_{max} + Z_{max})/\varepsilon$, contradicting the definition of δ_{max} in (3.26).

Proof of Theorem 2.2

Here we prove Theorem 2.2.

Proof 1). First, we prove $Q(t) \leq Q_{max}$ for every time slot t. Once again, we will use induction method. Obviously, $Q(0) \leq Q_{max}$. Suppose it holds at time slot t, we need to show that it also holds at time slot $t+1$. As $Q(t+1) = \max[Q(t)-D(t)-G_l(t), 0] + A_{ela}(t)$, if $Q(t) \leq V_{ela}C_{max}$, then the maximum amount of energy demand arrival is A_{ela}^{max}, we have $Q(t+1) \leq V_{ela}C_{max} + A_{ela}^{max}$. If $V_{ela}C_{max} < Q(t) \leq V_{ela}C_{max}+A_{ela}^{max}$, then $V_{ela}C(t)-Z(t)-Q(t) < 0$. According to **Problem Six**, our algorithm will choose $G_{l,ela}^{*}(t) = G_l^{max}$. If $Q(t) - D_{ela}^{*}(t) - G_l^{max} > 0$, then, in time slot t the amount of energy demand being served is at least G_l^{max}, which is larger than the maximum amount of arrival during time slot t. Hence, the queue cannot increase, i.e., $Q(t+1) \leq Q(t) \leq V_{ela}C_{max} + A_{ela}^{max}$. If $Q(t) - D_{ela}^{*}(t) - G_l^{max} \leq 0$, then $Q(t+1) = A_{ela}(t) \leq A_{ela}^{max} \leq V_{ela}C_{max} + A_{ela}^{max}$. Therefore, we have proved $Q(t) \leq V_{ela}C_{max} + A_{ela}^{max}$.

Next, we prove $Z(t) \leq Z_{max}$ for every time slot t. Obviously, $Z(0) \leq Z_{max}$. Suppose it holds for time slot t, we need to show that it also holds in time slot $t+1$. As $Z(t+1) = \max[Z(t)-D(t)-G_l(t)+\varepsilon 1_{Q(t)>0}, 0]$, if $Z(t) \leq V_{ela}C_{max}$, then the maximum amount of queuing increase is ε, we have $Z(t+1) \leq V_{ela}C_{max}+\varepsilon$; if $V_{ela}C_{max} < Z(t) \leq V_{ela}C_{max} + \varepsilon$, then $V_{ela}C(t) - Z(t) - Q(t) < 0$. According to **Problem Six**, our algorithm will choose $G_{l,ela}^{*}(t) = G_l^{max}$. If $Z(t) - D_{ela}^{*}(t) - G_l^{max} > 0$, then, in time slot t the amount of energy demand being served is at least G_l^{max}, which is larger than the maximum amount of arrival ε during time slot t. Hence, the queue cannot increase, i.e., $Z(t+1) \leq Z(t) \leq V_{ela}C_{max} + \varepsilon$. If $Z(t) - D_{ela}^{*}(t) - G_l^{max} \leq 0$, then $Z(t+1) \leq \varepsilon \leq V_{ela}C_{max} + \varepsilon$. Therefore, we have proved that $Z(t) \leq V_{ela}C_{max} + \varepsilon$.

Finally, we prove $Q(t) + Z(t) \leq \Theta_{max}$. Obviously, $Q(0) + Z(0) \leq \Theta_{max}$. Suppose $Q(t) + Z(t) \leq \Theta_{max}$ holds for time slot t. If $Q(t) + Z(t) \leq V_{ela}C_{max}$, then, according to the queuing equations of $Q(t)$ and $Z(t)$, the maximum increase during one slot is $A_{ela}^{max} + \varepsilon$. If $VC_{max} < Q(t) + Z(t) \leq V_{ela}C_{max} + A_{ela}^{max} + \varepsilon$, then $V_{ela}C(t) - Z(t) - Q(t) < 0$. According to **Problem Six**, our algorithm will choose $G_{l,ela}^{*}(t) = G_l^{max}$. Using the proof above, $U(t+1)$ and $Z(t+1)$ cannot increase. Hence, $U(t+1) + Z(t+1) \leq U(t) + Z(t) \leq \Theta_{max}$. This completes the proof for 1).

2). This is straightforward from Lemma 3.1.

3). It is obvious that the optimal solution to **Problem Six** has the following properties:

- If $X(t) > -V_{ela}C_{min}$, $G_{b,ela}^{*}(t) = 0$.
- If $X(t) < -[Q(t) + Z(t)]_{max} = -\Theta_{max}$, $D_{ela}^{*}(t) = 0$.

In the following, we prove this result by induction. When $t = 0$, as $X_{ela}(0) = B_0 - \Theta_{max} - D_{max}$ and $0 \leq B_0 \leq B_{max}$, we have $-\Theta_{max} - D_{max} \leq X(0) \leq B_{max} - \Theta_{max} - D_{max}$.

Now suppose that the above bound holds for time slot t. We need to show that it also holds for time slot $t+1$. First, suppose $0 < X_{ela}(t) \leq B_{max} - \Theta_{max} - D_{max}$, then $G^*_{b,ela}(t) = \gamma^*_{ela}(t) = 0$. As there is no recharge to the battery and the maximum discharge rate during one time slot is D_{max}, we have $-\Theta_{max} - D_{max} < -D_{max} < X_{ela}(t+1) \leq X_{ela}(t) \leq B_{max} - \Theta_{max} - D_{max}$. Second, suppose $-V_{ela}C_{min} < X_{ela}(t) \leq 0$, then $G^*_{b,ela}(t) = 0$ and the maximum recharge and discharge rate for the battery are S_{max} and D_{max}, respectively. Hence, $-\Theta_{max} - D_{max} < -V_{ela}C_{min} - D_{max} < X_{ela}(t+1) \leq X_{ela}(t) + S_{max} \leq B_{max} - \Theta_{max} - D_{max}$, where we have used

$$V_{ela} \leq \frac{B_{max} - A^{max}_{ela} - \varepsilon - D_{max} - G^{max}_b - S_{max}}{C_{max} - C_{min}},$$

and $V^{max}_{ela}C_{min} \leq G^{max}_b$. Third, suppose $-\Theta_{max} \leq X_{ela}(t) \leq -V_{ela}C_{min}$. As $X_{ela}(t) - D_{max} \leq X_{ela}(t+1) \leq X_{ela}(t) + S_{max} + G^{max}_b$, we have $-\Theta_{max} - D_{max} \leq X_{ela}(t+1) \leq -V_{ela}C_{min} + S_{max} + G^{max}_b \leq B_{max} - (V_{ela}C_{max} + A^{max}_{ela} + \varepsilon) - D_{max} = B_{max} - \Theta_{max} - D_{max}$, where we use the same bound of V_{ela} as the case before. Last, suppose $-\Theta_{max} - D_{max} \leq X(t) < -\Theta_{max}$, from **Problem Six**, we have $D^*_{ela}(t) = 0$, then $-\Theta_{max} - D_{max} \leq X_{ela}(t) \leq X_{ela}(t+1) < -\Theta_{max} + S_{max} + G^{max}_b \leq B_{max} - \Theta_{max} - D_{max}$. This completes the proof of 3).

4). From 3) and the definition (2.27) of $X_{ela}(t)$, it follows immediately that $0 \leq B(t) \leq B_{max}$ holds all slots t. Further, we choose our decisions to satisfy all constraints in **Problem Six**. Combining them together, all constraints of **Problem Four** are satisfied. Therefore, our control decisions are feasible to **Problem Four**.

5). Here, we make use of Lyapunov optimization techniques to derive this result. Denote queue states $\mathbf{K}(t) \triangleq (Q(t), Z(t), X_{ela}(t))$. Define the Lyapunov function as $L(\mathbf{K}(t)) = \frac{1}{2}(Q^2(t) + Z^2(t) + X^2_{ela}(t))$ and the conditional 1-slot Lyapunov drift as follows:

$$\triangle(\mathbf{K}(t)) = \mathbb{E}\{L(\mathbf{K}(t+1)) - L(\mathbf{K}(t))|\mathbf{K}(t)\}.$$

From the update Eq. (2.28), squaring both sides, we obtain

$$\frac{X^2_{ela}(t+1) - X^2_{ela}(t)}{2} = \frac{(D(t) - \gamma(t)S(t) - G_b(t))^2}{2} - X_{ela}(t)(D(t) - \gamma(t)S(t) - G_b(t)).$$

As $0 \leq D(t) \leq D_{max}$ and $0 \leq \gamma(t)S(t) + G_b(t) \leq G^{max}_b + S_{max}$, we have

$$\frac{(D(t) - \gamma(t)S(t) - G_b(t))^2}{2} \leq \frac{1}{2}\max[(G^{max}_b + S_{max})^2, D^2_{max}].$$

Therefore, we can get the following upper bound for the Lyapunov drift for $X(t)$:

$$\frac{X_{ela}^2(t+1) - X_{ela}^2(t)}{2} \leq \frac{1}{2}\max[(G_b^{max} + S_{max})^2, D_{max}^2] - X_{ela}(t)(D(t) - \gamma(t)S(t) - G_b(t)).$$

From the update Eq. (3.25), we have

$$Z(t+1) \leq \max[Z(t) - D(t) - G_l(t) + \varepsilon, 0],$$

then,

$$Z^2(t+1) \leq (Z(t) - D(t) - G_l(t) + \varepsilon)^2,$$

and we obtain the following inequality:

$$\begin{aligned}
&\frac{Z^2(t+1) - Z^2(t)}{2} \\
&\leq \frac{(\varepsilon - D(t) - G_l(t))^2}{2} + Z(t)(\varepsilon - D(t) - G_l(t)) \\
&\leq \frac{\max[(D_{max} + G_l^{max})^2, \varepsilon^2]}{2} + Z(t)(\varepsilon - D(t) - G_l(t)).
\end{aligned}$$

From the update Eq. (2.18), squaring both sides and using the following inequality:

$$\begin{aligned}
&(\max[Q(t) - D(t) - G_l(t), 0] + A_{ela}(t))^2 \leq A_{ela}^2(t) + \\
&Q^2(t) + (D(t) + G_l(t))^2 + 2Q(t)(A_{ela}(t) - D(t) - G_l(t)),
\end{aligned}$$

we obtain

$$\frac{Q^2(t+1) - Q^2(t)}{2} \leq \frac{[(D_{max} + G_l^{max})^2 + A_{ela,max}^2]}{2} + Q(t)(A_{ela}(t) - D(t) - G_l(t)).$$

Combining these three bounds together and taking the expectation w.r.t. $\mathbf{K}(t)$ on both sides, we arrive at the following inequality:

$$\begin{aligned}
\triangle(\mathbf{K}(t)) \leq & B_2 + \mathbb{E}\{Z(t)(\varepsilon - D(t) - G_l(t))|\mathbf{K}(t)\} \\
& + \mathbb{E}\{Q(t)(A_{ela}(t) - D(t) - G_l(t))|\mathbf{K}(t)\} \\
& - \mathbb{E}\{X_{ela}(t)(D(t) - \gamma(t)S(t) - G_b(t))|\mathbf{K}(t)\},
\end{aligned}$$

where $B_2 = \frac{\max[(S_{max}+G_b^{max})^2, D_{max}^2]}{2} + \frac{\max[(D_{max}+G_l^{max})^2, \varepsilon^2]}{2} + \frac{[(D_{max}+G_l^{max})^2 + A_{ela,max}^2]}{2}$. Adding penalty term $V_{ela}\mathbb{E}\{C(t)(G_l(t)+G_b(t))|\mathbf{K}(t)\}$ to both sides of the above inequality, we obtain the following inequality:

$$\begin{aligned}\triangle(\mathbf{K}(t)) + V_{ela}\mathbb{E}\{C(t)(G_l(t)+G_b(t))|\mathbf{K}(t)\} \le B_2 \\ - X_{ela}(t)\mathbb{E}\{D(t) - \gamma(t)S(t) - G_b(t)|\mathbf{K}(t)\} \\ + Z(t)\mathbb{E}\{\varepsilon - D(t) - G_l(t)|\mathbf{K}(t)\} \\ + Q(t)\mathbb{E}\{A_{ela}(t) - D(t) - G_l(t)|\mathbf{K}(t)\} \\ + V_{ela}\mathbb{E}\{C(t)(G_l(t)+G_b(t))|\mathbf{K}(t)\}.\end{aligned}$$

Comparing with the objective of **Problem Six**, it is obvious that our algorithm always attempts to greedily minimize the R.H.S. of the above inequality at each time slot t over all feasible control policies including the optimal, stationary policy given in Lemma 2.2. Plugging this policy $(\hat{D}_{ela}(t), \hat{G}_{l,ela}(t), \hat{G}_{b,ela}(t), \hat{\gamma}_{ela}(t))$ into the R.H.S. of the inequality above and using the fact that this policy is independent of queue state $\mathbf{K}(t)$, we obtain the following:

$$\begin{aligned}\triangle(\mathbf{K}(t)) + V_{ela}\mathbb{E}\{C(t)(G_l(t)+G_b(t))|\mathbf{K}(t)\} \le B_2 \\ - X_{ela}(t)\mathbb{E}\{\hat{D}_{ela}(t) - \hat{\gamma}_{ela}(t)S(t) - \hat{G}_{b,ela}(t)|\mathbf{K}(t)\} \\ + Z(t)\mathbb{E}\{\varepsilon - \hat{D}_{ela}(t) - \hat{G}_{l,ela}(t)|\mathbf{K}(t)\} \\ + Q(t)\mathbb{E}\{A_{ela}(t) - \hat{D}_{ela}(t) - \hat{G}_{l,ela}(t)|\mathbf{K}(t)\} \\ + V_{ela}\mathbb{E}\{C(t)(\hat{G}_{l,ela}(t) + \hat{G}_{b,ela}(t))|\mathbf{K}(t)\} \\ \le B_2 + V_{ela}P_{2,rel}^* \le B_2 + V_{ela}P_2^*,\end{aligned}$$

where the following facts have been used:

$$\mathbb{E}\{\hat{D}_{ela}(t) - \hat{\gamma}_{ela}(t)S(t) - \hat{G}_{b,ela}(t)|\mathbf{K}(t)\} = 0, \tag{2.36}$$

$$\mathbb{E}\{A_{ela}(t) - \hat{D}_{ela}(t) - \hat{G}_{l,ela}(t)|\mathbf{K}(t)\} \le 0, \tag{2.37}$$

$$\mathbb{E}\{\varepsilon - \hat{D}_{ela}(t) - \hat{G}_{l,ela}(t)|\mathbf{K}(t)\} \le 0. \tag{2.38}$$

The first two equations follow from Lemma 2.2 and the last one follows from (2.37) together with $\varepsilon \le \mathbb{E}\{A_{ela}(t)\}$. Taking the expectation on both sides, using the law of iterative expectation, and summing over $t \in \{0, 1, 2, \ldots, T-1\}$, we obtain

$$\begin{aligned}V_{ela}\sum_{t=0}^{T-1}\mathbb{E}\{C(t)(G_l(t)+G_b(t)) \le B_2T + V_{ela}TP_2^* \\ - \mathbb{E}\{L(\mathbf{K}(T))\} + \mathbb{E}\{L(\mathbf{K}(0))\}.\end{aligned}$$

Dividing both sides by T, letting $T \to \infty$, and using the facts that $E\{L(\mathbf{K}(0))\}$ are finite and $E\{L(\mathbf{K}(t))\}$ are nonnegative, we arrive at the following result for our algorithm:

$$\lim_{T\to\infty} \frac{1}{T} \sum_{t=0}^{T-1} \mathbb{E}\{C(t)(G_l(t) + G_b(t))\} \leq P_2^* + B_2/V_{ela},$$

where P_2^* is the optimal objective value, B_2 is a constant given by Eq. (2.34), and V_{ela} is a tunable control parameter which has a maximum value given by Eq. (2.29). This completes the proof.

References

1. Rahul Urgaonkar, Bhuvan Urgaonkary, Michael J. Neely, and Anand Sivasubramaniam. Optimal power cost management using stored energy in data centers. In *ACM International Conference on Measurement and Modeling of Computer Systems, SIGMETRICS 2011*, SAN JOSE, June 2011.
2. Aman Kansal, Jason Hsu, Sadaf Zahedi, and Mani B. Srivastava. Power management in energy harvesting sensor networks. *ACM Trans. Embed. Comput. Syst.*, 6, September 2007.
3. D. Linden and T. B. Reddy. *Handbook of Batteries*. McGraw Hill Handbooks, 2002.
4. Asfandyar Qureshi, Rick Weber, Hari Balakrishnan, John Guttag, and Bruce Maggs. Cutting the electric bill for internet-scale systems. In *ACM SIGCOMM*, Barcelona, Spain, August 2009.
5. Amir-Hamed Mohsenian-Rad and Alberto Leon-Garci. Energy-information transmission tradeoff in green cloud computing. In *Proc. of IEEE Global telecommunications conference, Globecom'10*, Miami, March 2010.
6. Leonidas Georgiadis, Michael J. Neely, and Leandros Tassiulas. *Resource allocation and cross-layer control in wireless networks*, volume 1. Now Publishers Inc., 2006.
7. M. J. Neely. *Stochastic Network Optimization with Application to Communication and Queueing Systems*. Morgan Claypool, 2010.
8. Dimitri P. Bertsekas. *Dynamic Programming and Optimal Control*. Athena Scientific, 2nd edition, 2000.
9. Longbo Huang and Michael J. Neely. Utility optimal scheduling in energy harvesting networks. In *MobiHoc, 2011 ACM International Symposium on Mobile Ad Hoc Networking and Computing*, May 2011.
10. M.J. Neely, A.S. Tehrani, and A.G. Dimakis. Efficient algorithms for renewable energy allocation to delay tolerant consumers. In *Smart Grid Communications (SmartGridComm), 2010 First IEEE International Conference on*, oct. 2010.
11. California ISO Open Access Same-time Information System (OASIS).
12. NREL: Measurement and Instrumentation Data Center.

Chapter 3
Decentralized Coordination of Energy Consumption for Smart Neighborhoods

3.1 System Model

Consider a set of N smart homes or households that are served by a single load serving entity (LSE) in a neighborhood setting. The LSE may be a utility company and the neighborhood would cover all households connected to a step-down transformer in the distribution network connected to the electric grid. The LSE participates into wholesale electricity markets (day-ahead, hour-ahead, real-time balancing, ancillary service) to purchase electricity from power generators and then sell it to the N customers in the retail market. Currently, the electricity price in the retail market is usually flat because of the simplicity and predictability. However, it does not encourage efficient usage of electricity, causing high peak demand and low load factor. We consider coordinated energy management of multiple smart homes in a neighborhood for more efficient energy utilization so as to benefit both customers and the whole power system. A schematic diagram of a smart neighborhood is shown in Fig. 3.1.

In this section, we first provide mathematical descriptions for LSE, energy loads, energy storage, and distributed renewable generation in smart homes. Based on these definitions, we then formulate our control problem as a stochastic programming in Sect. 3.2. We consider a time-slotted model with an infinite horizon. Each slot represents a suitable period for control decisions (e.g., 15 min) and is indexed by $t = \{0, 1, \ldots\}$.

3.1.1 Load Serving Entity

The LSE serves as an agent that is responsible for purchasing enough electricity from wholesale electricity markets to serve the energy demand of the households

Y. Guo et al., *Stochastic Optimization for Distributed Energy Resources in Smart Grids*, SpringerBriefs in Electrical and Computer Engineering,
DOI 10.1007/978-3-319-59529-0_3

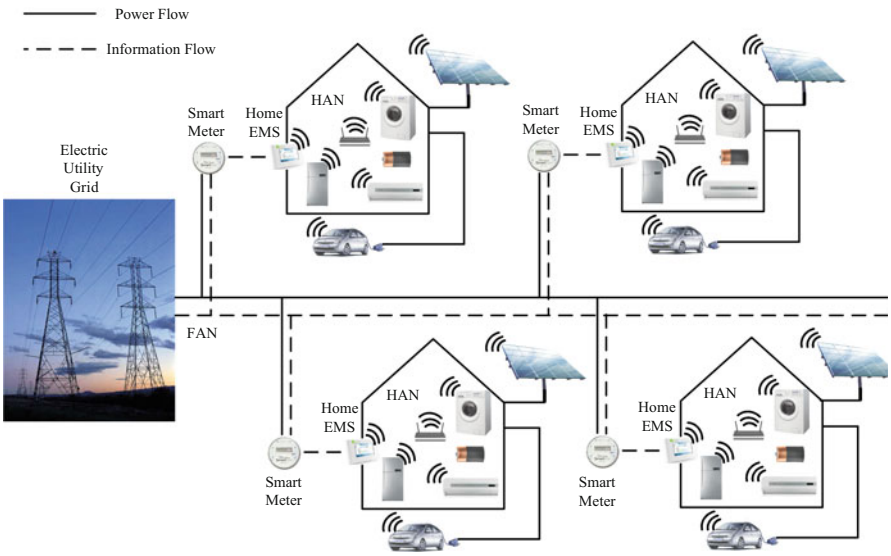

Fig. 3.1 Schematic of household energy management in a neighborhood

in its service area. The retail price is set in order to at least recover the running cost of the LSE. In future smart grids, field area network (FAN) would be deployed, which can provide convenient communications between utility companies and smart meters of residential households. For simplicity, we make the following assumption that the cost of the LSE can be represented by a time-varying cost function $C_t(D)$ that specifies the cost when providing amount D of electricity to the N customers at time slot t. Here, we only assume that the cost function $C_t(D)$ is a increasing, continuously differentiable, and convex in D for any t with a bounded first derivative. We use α^{min} and α^{max} to denote the minimum and the maximum first derivatives of $C_t(D)$, respectively. That is, $\alpha^{min} \leq (C_t)' \leq \alpha^{max}$.

3.1.2 Energy Loads

In general, the energy loads in a home can be roughly divided into two categories: inelastic and elastic loads. Examples of inelastic energy loads include lights, TVs, microwaves, and computers. For this type of energy loads, the energy requests must be met exactly at the time t when needed. In contrast, there are some energy loads, i.e., smart appliances, in homes that are elastic in the sense that they can be controlled to adjust the times of their operations and the amount of their energy usage without impacting the satisfaction of customers. In other words, as long as their energy requirements are met within certain deadlines, the household occupants would be satisfied. Examples include refrigerators, dehumidifiers, air conditioning,

and charging of some PHEVs. Actually, the vast majority of household loads are inelastic. However, as observed in [1], while the elastic energy loads comprise less than 7.5% of the total loads in a household, they account for 59% of the average energy consumption. Therefore, it would be significant to schedule the energy consumption of these elastic energy loads so as to achieve certain objective such as minimizing the electricity bill or the peak demand.

Inside a household, electric appliances can communicate with the smart meter via the home area network (HAN), which may be Wi-Fi or ZigBee. For each home $i \in N$, denote by $d_{i,1}(t)$ the inelastic energy loads (in unit of kWh) and by $d_{i,2}(t)$ the elastic energy loads (in unit of kWh) at time t. Assume that the elastic energy loads are "buffered" (i.e., the energy requests are held or delayed) first in a queue $Q_i(t)$ before being served. Denote by $y_i(t)$ the energy amount that is used for serving the queued energy loads at time t. Then the dynamics of $Q_i(t)$ is as follows:

$$Q_i(t+1) = \max\{Q_i(t) - y_i(t), 0\} + d_{i,2}(t), \quad \forall i. \tag{3.1}$$

For any feasible control decision, we need to ensure that the average delay of the elastic loads in the queue is finite. In other words, we cannot delay arbitrarily long time for the service of elastic energy loads. This can be stated as follows:

$$\overline{Q_i} \doteq \limsup_{T\to\infty} \frac{1}{T} \sum_{t=0}^{T-1} \mathbb{E}\{Q_i(t)\} < \infty. \tag{3.2}$$

3.1.3 Energy Storage

In addition to energy loads, each household may have some kind of energy storage facility, possibly in the form of the battery in PHEV. For each household i, we denote by E_i^{max}, the battery capacity, by $E_i(t)$, the energy level of the battery at time t, and by $r_i(t)$, the power charged to (when $r_i(t) > 0$) or discharged from (when $r_i(t) < 0$) the battery during slot t. Assume that the battery energy leakage is negligible and batteries at households operate independently of each other. Then we model the dynamics of the battery energy level by[1]

$$E_i(t+1) = E_i(t) + r_i(t). \tag{3.3}$$

For each household i, the battery usually has an upper bound on the charge rate, denoted by r_i^{max}, and an upper bound on the discharge rate, denoted by $-r_i^{min}$, where

[1] In this chapter, all power quantities such as $r_i(t)$, $s_i(t)$, $y_i(t)$, $d_{i,1}(t)$, $d_{i,2}(t)$ are in the unit of energy per slot, so the energy produced/consumed in time period t are $r_i(t)$, $s_i(t)$, $y_i(t)$, $d_{i,1}(t)$, $d_{i,2}(t)$, respectively.

r_i^{max} and $-r_i^{min}$ are positive constants depending on the physical properties of the battery. Therefore, we have the following constraint on $r_i(t)$:

$$r_i^{min} \leq r_i(t) \leq r_i^{max}. \tag{3.4}$$

The battery energy level should be always nonnegative and cannot exceed the battery capacity. So in each time slot t, we need to ensure that for each household i,

$$0 \leq E_i(t) \leq E_i^{max}. \tag{3.5}$$

From constraints (3.3), (3.4), and (3.5), we obtain the following equivalent constraints in each slot t at household i:

$$r_i(t) \geq \min\{r_i^{min}, -E_i(t)\}, \tag{3.6}$$

$$r_i(t) \leq \min\{r_i^{max}, E_i^{max} - E_i(t)\}. \tag{3.7}$$

However, the cost of battery use cannot be ignored. In practice, there are limited times of charging/discharing cycles for each battery. Besides, conversion loss occurs both in charging and discharging processes. Stored energy is also subject to leakage with time. All these factors depend on how fast/much/often it is charged and discharged. Instead of modeling these factors exactly, we use an amortized time-invariant cost function $F_i(r_i)$ (in unit of dollars) to model the impact of charging or discharging operation r_i on the battery during one slot for household i. Each battery cost function $F_i(r_i)$ is assumed to be increasing, continuously differentiable, and convex in r_i with a bounded first derivative and $F_i(0) = 0$. We use β_i^{min} and β_i^{max} to denote the minimum and the maximum first derivatives of $F_i(r_i)$ for each household i, respectively. That is, $\beta_i^{min} \leq (F_i)' \leq \beta_i^{max}, \forall i$.

3.1.4 Renewable Distributed Generation

Due to the environmental concern as well as decreasing cost for renewable generation, each household i may possess a distributed renewable generator installed on its site, such as rooftop PV panel or small wind turbine. Denote by $s_i(t)$ the renewable energy generated in slot t by the renewable distributed generation (DG), which largely depends on weather information in the environment and is usually intermittent, unpredictable, and uncontrollable. In this chapter, we assume it is i.i.d. across different slots and has the maximum value given by its rated power s_i^{max}. Therefore, we have

$$0 \leq s_i(t) \leq s_i^{max} \quad \forall i, t. \tag{3.8}$$

Note that the energy generation density of a renewable generator is usually lower than the normal energy consumption density of households. Households need to

connect to the utility electric grid for backup power and, therefore, are mostly grid-tied systems. Here, we assume that the renewable energy is free and should be utilized as much as possible.

3.2 Problem Formulation

With the above models for the battery and distributed renewable generator, at each time t, the total power demand of household i needed from the utility electric grid is

$$g_i(t) \doteq \max\{d_{i,1}(t) + y_i(t) + r_i(t) - s_i(t), 0\}. \tag{3.9}$$

Note that we have assumed that power cannot be fed from the household into the utility electric grid in the formula above.

In this chapter, we are interested in minimizing the time-average total energy cost of the whole neighborhood, or the negative of social welfare, which equals to the generation cost plus the battery cost. Therefore, the control problem is that: for the dynamic system defined by (3.1) and (3.3), design a control strategy which, given the past and present random renewable supplies, the battery energy levels, the energy demands, and the energy cost function, chooses the battery charge/discharge vector $\mathbf{r}$ and the elastic load serving rate vector $\mathbf{y}$ such that the time-average total energy cost of the whole neighborhood is minimized. It can be formulated as the following stochastic programming problem, called **P1**:

$$\min_{\mathbf{y},\mathbf{r}} : \limsup_{T\to\infty} \frac{1}{T} \sum_{t=0}^{T-1} \mathbb{E}\{C_t(\sum_{i=1}^{N} g_i(t)) + \sum_{i=1}^{N} F_i(r_i(t))\}, \tag{3.10}$$

s.t.

$$r_i(t) \geq \min\{r_i^{min}, -E_i(t)\}, \quad \forall i, t, \tag{3.11}$$

$$r_i(t) \leq \min\{r_i^{max}, E_i^{max} - E_i(t)\}, \quad \forall i, t, \tag{3.12}$$

$$y_i(t) \geq 0, \quad \forall i, t, \tag{3.13}$$

$$\overline{Q_i} < \infty, \quad \forall i. \tag{3.14}$$

Here the expectation in the objective is w.r.t. the random renewable generation $s_i(t)$, the random inelastic energy loads $d_{i,1}(t)$, the random elastic energy loads $d_{i,2}(t)$ for each household, and the random cost function C_t.

3.3 Online Distributed Algorithm

In this section, we design algorithms to solve **P1**. One challenge of solving the stochastic optimization problem above is the uncertainty of future renewable generation, time-varying cost function, inelastic or elastic energy loads. Moreover, the constraints on $E_i(t)$ bring the "time-coupling" property to the stochastic optimization problem above. That is to say, the current control action may impact the future control actions, making it more challenging to solve. Our solution is based on the technique of Lyapunov optimization [2] and requires minimum information on the random dynamics in the system. To carry out our design, we first consider a related problem and obtain a lower bound on the optimal operation cost of **P1**, which is useful for our later analysis. After that, we will describe our proposed online algorithms to approximately solve it.

3.3.1 Relaxed Problem

Before presenting the solution to **P1**, we first consider a relaxed problem. Define the time-average expected value of battery charge/discharge rate for household i under any feasible control policy of **P1** as follows:

$$\overline{r_i} = \limsup_{T\to\infty} \frac{1}{T} \sum_{t=0}^{T-1} \mathbb{E}\{r_i(t)\}. \tag{3.15}$$

Since the dynamics of battery energy level is (3.3), summing over all $t \in \{0, 1, \ldots, T-1\}$, and taking expectation of both sides, we obtain

$$\mathbb{E}\{E_i(T)\} - E_i(0) = \sum_{t=0}^{T-1} \mathbb{E}\{r_i(t)\}. \tag{3.16}$$

As $0 \le E_i(t) \le E_i^{max}$ for all slots t, dividing both sides by T, and taking $T \to \infty$ yields $\overline{r_i} = 0$. Hence we have the following relaxed problem, called **P2**:

$$\min_{\mathbf{y},\mathbf{r}} : \limsup_{T\to\infty} \frac{1}{T} \sum_{t=0}^{T-1} \mathbb{E}\left\{ C_t\left(\sum_{i=1}^{N} g_i(t)\right) + \sum_{i=1}^{N} F_i(r_i(t))\right\}, \tag{3.17}$$

s.t.

$$r_i^{min} \le r_i(t) \le r_i^{max}, \quad \forall i, t, \tag{3.18}$$

$$\overline{r_i} = 0, \quad \forall i, \tag{3.19}$$

$$y_i(t) \ge 0, \quad \forall i, t, \tag{3.20}$$

$$\overline{Q_i} < \infty, \quad \forall i. \tag{3.21}$$

Denote by **P1*** the optimal objective value of **P1** and by **P2*** the optimal objective value of **P2**, respectively. Since any feasible solution to **P1** is also a feasible solution to **P2**, **P2**$^* \leq$ **P1***. Note that **P2** is a decoupled control problem since no correlation exists in any constraint. From the framework of Lyapunov optimization [2], we have the following theorem for the solution to **P2**:

Theorem 3.1 *If $s_i(t)$, $d_{i,1}(t)$, $d_{i,2}(t)$, and $C_t(\cdot)$ are i.i.d. over slots, then there exists a stationary, randomized policy that takes control decisions $\mathbf{y}^{stat}$ and $\mathbf{r}^{stat}$ every slot purely as a function (possibly randomized) of the current system status while satisfying the constraints of **P2** and providing the following guarantees:*

$$\mathbb{E}\{r_i^{stat}(t)\} = 0, \quad \forall i, \tag{3.22}$$

$$\mathbb{E}\{y_i^{stat}(t)\} \geq \mathbb{E}\{d_{i,2}(t)\}, \quad \forall i, \tag{3.23}$$

$$\mathbb{E}\left\{C_t\left(\sum_{i=1}^{N} g_i^{stat}(t)\right) + \sum_{i=1}^{N} F_i(r_i^{stat}(t))\right\} = \boldsymbol{P2}^*, \tag{3.24}$$

where the expectation in the objective is w.r.t. the random renewable generation $s_i(t)$, the random inelastic energy loads $d_{i,1}(t)$, the random elastic energy loads $d_{i,2}(t)$ for each household, and the random cost function C_t.

Proof It can be proven using Caratheodory's theorem as shown in [2, 3] and is similar to that in [4]. It is omitted here for brevity.

In order to derive such a stationary policy, we need to know the statistical distributions of all combinations of $s_i(t)$, $d_{i,1}(t)$, $d_{i,2}(t)$, and $C_t(\cdot)$, which usually has the problem of "curse of dimensionality" [5] if solved by dynamic programming. Moreover, this control policy may not be a feasible solution to **P1**. Instead, we use the existence of such a policy to help us design our control policy that meets all constraints of **P1** and derive the analytical performance of our algorithm as illustrated in the proof of our algorithm performance properties later.

3.3.2 Delay-Aware Virtual Queue

Since the constraint $\overline{Q_i} < \infty$ only ensures finite average delay for the elastic energy loads in household i, worst-case delay guarantee is usually desired in practice. For this purpose, we leverage the technique of $\varepsilon-$ persistent queue. Specifically, the following virtual queues $Z_i(t), i = 1, 2, \ldots, N$ are defined to provide the worst-case delay guarantee on any buffered elastic energy loads in $Q_i(t)$:

$$Z_i(t+1) = \max\{Z_i(t) - y_i(t) + \varepsilon_i 1_{\{Q_i(t)>0\}}, 0\}, \tag{3.25}$$

where $1_{\{Q_i(t)>0\}}$ is an indicator function that is 1 if $Q_i(t) > 0$ or 0 otherwise; ε_i is a fixed positive parameter to be specified later. The intuition behind this virtual queue

is that since $Z_i(t)$ has the same service process as $Q_i(t)$, but has an arrival process that adds ε_i whenever the actual backlog is nonempty, this ensures that $Z_i(t)$ grows if there are energy loads in the queue $Q_i(t)$ that have not been serviced for a long time. The following lemma shows that if we can control the system to ensure that the queues $Q_i(t)$ and $Z_i(t)$ have finite upper bounds, then any buffered energy load is served within a worst-case delay as follows:

Lemma 3.1 *Suppose we can control the system to ensure that* $Z_i(t) \leq Z_i^{max}$ *and* $Q_i(t) \leq Q_i^{max}$ *for all slots t, where* Z_i^{max} *and* Q_i^{max} *are some positive constants. Then, the worst-case delay for all buffered energy loads in household i is upper bounded by* δ_i^{max} *slots where*

$$\delta_i^{max} \triangleq \lceil \frac{(Q_i^{max} + Z_i^{max})}{\varepsilon_i} \rceil. \tag{3.26}$$

Proof The proof follows directly from the framework of Lyapunov optimization [2] and is given in Appendix 3.5.2 for completeness.

We will show that there indeed exist such constants Z_i^{max} and Q_i^{max} for all households i later.

3.3.3 The Lyapunov Approach

The idea of our algorithm is to construct a Lyapunov-based scheduling algorithm with perturbed weights for determining the optimal power usage. By carefully perturbing the weights, we can ensure that whenever we charge or discharge the battery, the energy level in the battery always lies in the feasible region.

First, we choose a perturbation vector $\boldsymbol{\theta} = (\theta_i, \ \forall i)$ (to be specified later). We define a perturbed Lyapunov function as follows:

$$L(t) \doteq \frac{1}{2} \sum_{i=1}^{N} [(E_i(t) - \theta_i)^2 + Q_i^2(t) + Z_i^2(t)]. \tag{3.27}$$

Now define $\mathbf{K}(t) = (\mathbf{Q}(t), \mathbf{Z}(t), \mathbf{E}(t))$, and define a one-slot conditional Lyapunov drift as follows:

$$\triangle(t) = \mathbb{E}\{L(t+1) - L(t) \mid \mathbf{K}(t)\}. \tag{3.28}$$

Here the expectation is taken over the randomness of load arrivals, cost function, and renewable generation, as well as the randomness in choosing the control actions. Then, following the Lyapunov optimization framework, we add a function of the expected cost over one slot (i.e., the penalty function) to (3.28) to obtain the following *drift-plus-penalty* term:

$$\triangle_V(t) \doteq \triangle(t) + V\mathbb{E}\left\{ C_t\left(\sum_{i=1}^{N} g_i(t)\right) + \sum_{i=1}^{N} F_i(r_i(t)) \mid \mathbf{K}(t)\right\}, \tag{3.29}$$

where V is a positive control parameter to be specified later. Then, we have the following lemma regarding the *drift-plus-penalty* term:

Lemma 3.2 *Under any feasible action that can be implemented at slot t, we have*

$$\begin{aligned}\triangle_V(t) \le B &+ \sum_{i=1}^{N} \mathbb{E}\{(E_i(t) - \theta_i) r_i(t) \mid \mathbf{K}(t)\} \\ &+ \sum_{i=1}^{N} \mathbb{E}\{Q_i(t)(d_{i,2}(t) - y_i(t)) \mid \mathbf{K}(t)\} \\ &+ \sum_{i=1}^{N} \mathbb{E}\{Z_i(t)(\varepsilon_i - y_i(t)) \mid \mathbf{K}(t)\} \\ &+ V\mathbb{E}\left\{C_t\left(\sum_{i=1}^{N} g_i(t)\right) + \sum_{i=1}^{N} F_i(r_i(t)) \mid \mathbf{K}(t)\right\}, \end{aligned} \tag{3.30}$$

where B is a constant given by

$$\begin{aligned} B \doteq \sum_{i=1}^{N} \Big\{ &\frac{\max\{(r_i^{min})^2, (r_i^{max})^2\}}{2} + \frac{\max\{(y_i^{max})^2, \varepsilon_i^2\}}{2} \\ &+ \frac{(y_i^{max})^2 + (d_{i,2}^{max})^2}{2} \Big\}. \end{aligned} \tag{3.31}$$

Proof From (3.3), subtracting both sides by θ_i, and squaring both sides, we have for each household i,

$$\frac{(E_i(t+1) - \theta_i)^2 - (E_i(t) - \theta_i)^2}{2} = \frac{r_i^2(t)}{2} + r_i(t)(E_i(t) - \theta_i).$$

Moreover, we have the following inequality:

$$\frac{r_i^2(t)}{2} \le \frac{\max\{(r_i^{max})^2, (r_i^{min})^2\}}{2}.$$

Taking expectations of both sides of (3.3) given $\mathbf{K}(t)$, and summing over all households i, we can get the following upper bound for the Lyapunov drift for $E_i(t) - \theta_i$:

$$\begin{aligned} \frac{(E_i(t+1) - \theta_i)^2 - (E_i(t) - \theta_i)^2}{2} \le &\frac{\max\{(r_i^{max})^2, (r_i^{min})^2\}}{2} \\ &+ r_i(t)(E_i(t) - \theta_i). \end{aligned}$$

Also, from (3.1), squaring both sides, and using the following inequality:

$$(\max\{Q_i(t) - y_i(t), 0\} + d_{i,2}(t))^2 \leq d_{i,2}^2(t) + Q_i^2(t) + y_i^2(t) + 2Q(t)(d_{i,2}(t) - y_i(t)),$$

we obtain

$$\frac{Q_i^2(t+1) - Q_i^2(t)}{2} \leq \frac{(y_i^{max})^2 + (d_{i,2}^{max})^2}{2} + Q_i(t)(d_{i,2}(t) - y_i(t)).$$

Similarly, from (3.25), we have

$$Z_i^2(t+1) \leq (Z_i(t) - y_i(t) + \varepsilon_i)^2.$$

Then, we obtain the following inequality:

$$\begin{aligned} &\frac{Z_i^2(t+1) - Z_i^2(t)}{2} \\ &\leq \frac{(\varepsilon_i - y_i(t))^2}{2} + Z_i(t)(\varepsilon_i - y_i(t)) \\ &\leq \frac{\max\{(y_i^{max})^2, \varepsilon_i^2\}}{2} + Z_i(t)(\varepsilon_i - y_i(t)). \end{aligned}$$

Combining these three bounds together, taking the expectation w.r.t. $\mathbf{K}(t)$ on both sides, and adding penalty term $V\mathbb{E}\{C_t(\sum_{i=1}^N g_i(t)) + \sum_{i=1}^N F_i(r_i(t)) \mid \mathbf{K}(t)\}$ to both sides of the above inequality, we arrive at the conclusion in the lemma.

We now present our algorithm. The main design principle of our algorithm is to choose control actions that approximately minimize the R.H.S. of (3.30) subject to the constraints in **P2**. The intuition behind our algorithm is trying to store excess renewable energy for later use, recharge the battery during the period of low electricity price while discharging it during the period of high electricity price, and delay elastic energy loads to later slots with lower electricity price. Our algorithm is described in Algorithm 3. Note that the algorithm only requires the knowledge of the instant values of system dynamics and does not require any knowledge of the statistics of these stochastic processes. However, the algorithm above should be able to run distributively in order to be implemented in practice. In the ensuing subsection, we design a distributed algorithm to solve **P3**.

foreach *Time slot t* **do**

Observe the system states C_t, $d_{i,1}(t)$, $d_{i,2}(t)$, $s_i(t)$, and $\mathbf{K}(t)$;

Choose control decisions $\mathbf{y}^*$ and $\mathbf{r}^*$ as the optimal solution to the following optimization problem, called **P3**:

$$\min : \sum_{i=1}^{N} \Big\{ (E_i(t) - \theta_i) r_i(t) + VF_i(r_i(t)) - (Q_i(t) + Z_i(t)) y_i(t) \Big\} + VC_t(\sum_{i=1}^{N} g_i(t)),$$

s.t.

$$r_i^{min} \le r_i(t) \le r_i^{max}, \quad \forall i,$$
$$0 \le y_i(t) \le y_i^{max}, \quad \forall i.$$

Update $\mathbf{K}(t)$ according to the dynamics (3.1), (3.3), and (3.25);

end

Algorithm 3: The Lyapunov-based Cost Minimization Algorithm (LCMA)

3.3.4 Distributed Algorithm

First, we introduce the following ancillary variables: $h_i(t), \forall i$ to upper bound individual grid power demand and $D(t)$ to upper bound the total grid power demand. Then, we can transform **P3** into the following formulation, called **P4**:

$$\min_{\mathbf{y},\mathbf{r},\mathbf{h}} : \sum_{i=1}^{N} \Big\{ (E_i(t) - \theta_i) r_i(t) + VF_i(r_i(t)) - (Q_i(t) + Z_i(t)) y_i(t) \Big\} + VC_t(D(t)),$$

s.t.

$$r_i^{min} \le r_i(t) \le r_i^{max}, \quad \forall i,$$
$$0 \le y_i(t) \le y_i^{max}, \quad \forall i,$$
$$h_i(t) \ge d_{i,1}(t) + y_i(t) + r_i(t) - s_i(t), \quad \forall i, ,$$
$$0 \le h_i(t) \le h_i^{max}, \quad \forall i,$$
$$\sum_{i=1}^{N} h_i(t) \le D(t) \le D^{max},$$

Initialization: *Set* $\lambda_i^{(0)}(t), \forall i$, $\nu^{(0)}(t)$ *equal to some nonnegative value,* $k = 0$

foreach *Iteration* k **do**

  while *Not satisfying termination criterion* **do**

    Each household i updates $r_i^{(k)}(t)$, $y_i^{(k)}(t)$, and $h_i^{(k)}(t)$ after receiving the Lagrangian multiplier $\nu^{(k)}(t)$ according to the solution to the following optimization problem:

$$\min : (E_i(t) - \theta_i) r_i(t) + VF_i(r_i(t)) + \nu^{(k)}(t) h_i(t) - (Q_i(t) + Z_i(t)) y_i(t),$$

s.t.

$$h_i(t) - y_i(t) - r_i(t) \geq d_{i,1}(t) - s_i(t),$$
$$0 \leq h_i(t) \leq h_i^{max},$$
$$r_i^{min} \leq r_i(t) \leq r_i^{max},$$
$$0 \leq y_i(t) \leq y_i^{max}.$$

    The LSE collects the predictions of total utility power demands $\sum_{i=1}^{N} h_i^k(t)$ from all households i over the FAN. Then, it solves the optimal generation power and update the Lagrange multiplier as follows:

$$D^{(k)}(t) = \underset{0 \leq D(t) \leq D^{max}}{\operatorname{argmin}} \; VC_t(D(t)) - \nu^{(k)}(t) D(t), \tag{3.32}$$

$$\nu^{(k+1)}(t) = [\nu^{(k)}(t) - \alpha(D^{(k)}(t) - \sum_{i=1}^{N} h_i^{(k)}(t))]^+, \tag{3.33}$$

    where $\alpha > 0$ is a constant step-size, and then, broadcasts $\nu^{(k+1)}(t)$ to all households over the FAN

    Set $k \leftarrow k + 1$

  end

end

Algorithm 4: Distributed Algorithm to **P3**

where the maximum grid power consumption h_i^{max} is imposed because of security and reliability considerations for household i. Since $C_t(\cdot)$ is a strictly increasing function, we can easily prove by contradiction that the formulation above and **P3** are equivalent and have exactly the same optimal solutions in terms of $\mathbf{r}^*$ and $\mathbf{y}^*$. Since **P4** is a convex optimization problem and has decomposability structures, it motivates us to design the following distributed subgradient-based algorithm to iteratively solve it.

In each time slot t, the algorithm works as indicated in Algorithm 4. When the constant step-size α is small enough, the algorithm above converges to the optimal solution [6]. Note that other types of step-size can also be used with different convergence properties [7]. The algorithm is actually a standard dual decomposition algorithm, which has been extensively investigated in network utility maximization

problem in communication networks [8]. The proof of the correctness of this algorithm can be found in standard textbooks [7] and is omitted here for brevity. A desirable feature of our distributed algorithm is that the LSE does not need to know the detailed information about the energy usage in each individual household and only requires the total grid energy usage for all N households. By operating in this manner, our algorithm can help preserve the privacy of homeowners, who are shown to be concerned with some privacy issues associated with smart grids [9].

3.4 Performance Analysis

In this section, we analyze the performance of LCMA under the case that when the cost function $C_t(\cdot)$, renewable energy generation $s_i(t), \forall i$, energy load arrival processes $d_{i,1}(t), \forall i$ and $d_{i,2}(t), \forall i$ are all i.i.d., Note that our results can also be extended to the more general setting where $C_t(\cdot)$, $s_i(t), \forall i$, $d_{i,1}(t), \forall i$, and $d_{i,2}(t), \forall i$ all evolve according to some finite state irreducible and aperiodic Markov chains according to the Lyapunov optimization framework [2]. It is omitted here for brevity.

Theorem 3.2 *If $Q_i(0) = Z_i(0) = 0$ and $\theta_i = V(\alpha^{max} + \beta_i^{max}) - r_i^{min}$ for all households i, then under the LCMA algorithm for any fixed parameters $0 \leq \varepsilon_i \leq \mathbb{E}\{d_{i,2}(t)\}$, and $0 < V \leq V^{max}$, where*

$$V^{max} \doteq \min_i \frac{E_i^{max} - r_i^{max} + r_i^{min}}{\alpha^{max} + \beta_i^{max} - \alpha^{min} - \beta_i^{min}}, \tag{3.34}$$

we have the following properties:

1. *The queues $Q_i(t)$ and $Z_i(t)$ are deterministically upper bounded by Q_i^{max} and Z_i^{max} at every slot, where*

$$Q_i^{max} \doteq V\alpha^{max} + d_{i,2}^{max}, \tag{3.35}$$

$$Z_i^{max} \doteq V\alpha^{max} + \varepsilon_i. \tag{3.36}$$

   Further, $Q_i(t) + Z_i(t)$ are upper bounded by Θ_i^{max} where

$$\Theta_i^{max} \doteq V\alpha^{max} + d_{i,2}^{max} + \varepsilon_i. \tag{3.37}$$

2. *The worst-case delay of any buffered elastic energy load is given by:*

$$\delta_i^{max} = \lceil \frac{2V\alpha^{max} + d_{i,2}^{max} + \varepsilon_i}{\varepsilon_i} \rceil. \tag{3.38}$$

3. *The energy queue $E_i(t)$ satisfies the following for all time slots t:*

$$0 \leq E_i(t) \leq E_i^{max}. \tag{3.39}$$

4. *All control decisions are feasible.*
5. *If* $C_t(\cdot)$, $s_i(t), \forall i$, $d_{i,1}(t), \forall i$, *and* $d_{i,2}(t), \forall i$ *are i.i.d. over slots, then the time-average expected operating cost under our algorithm is within bound* B/V *of the optimal value, i.e.,*

$$\limsup_{T\to\infty} \frac{1}{T}\sum_{t=0}^{T-1}\mathbb{E}\left\{C_t\left(\sum_{i=1}^{N} g_i(t)\right)+\sum_{i=1}^{N} F_i(r_i(t))\right\} \leq \boldsymbol{P1}^* + B/V, \tag{3.40}$$

where B *is the constant specified in* (3.31).

Proof For each household i and time slot t,

1. First, we prove $Q_i(t) \leq Q_i^{max}$ for every time slot t. Once again, we will use induction method. Obviously, $Q_i(0) \leq Q_i^{max}$. Suppose it holds at time slot t, we need to show that it also holds at time slot $t+1$. As $Q_i(t+1) = \max\{Q_i(t) - y_i(t), 0\} + d_{i,2}(t)$, if $Q_i(t) \leq V\alpha^{max}$, and the maximum amount of inelastic energy load arrival is $d_{i,2}^{max}$, we have $Q_i(t+1) \leq V\alpha^{max} + d_{i,2}^{max}$. If $V\alpha^{max} < Q_i(t) \leq V\alpha^{max} + d_{i,2}^{max}$, LCMA will choose the maximum possible value for $y_i(t)$ since the partial derivative of the objective function in **P3** w.r.t. $y_i(t)$ is negative. If $Q_i(t) - y_i^*(t) > 0$, then, in time slot t the amount of energy demand being served is at least y_i^{max}, which is larger than the maximum amount of arrival during time slot t. Hence, the queue cannot increase, i.e., $Q_i(t+1) \leq Q_i(t) \leq V\alpha^{max} + d_{i,2}^{max}$. If $Q(t) - y_i^*(t) \leq 0$, then $Q_i(t+1) \leq d_{i,2}^{max} \leq V\alpha^{max} + d_{i,2}^{max}$. Therefore, we have proved $Q_i(t) \leq Q_i^{max}$.

   Next, we prove $Z_i(t) \leq Z_i^{max}$ for every time slot t. Obviously, $Z_i(0) \leq Z_i^{max}$. Assuming that it holds for time slot t, we need to show that it also holds in time slot $t+1$. As $Z_i(t+1) = \max\{Z_i(t) - y_i(t) + \varepsilon_i 1_{Q_i(t)>0}, 0\}$, if $Z_i(t) \leq V\alpha^{max}$, then the maximum amount of queuing increase is ε_i. We have $Z_i(t+1) \leq V\alpha^{max} + \varepsilon_i$; if $V\alpha^{max} < Z(t) \leq V\alpha^{max} + \varepsilon_i$, then LCMA will choose the maximum possible value for $y_i(t)$ since the partial derivative of the objective function in **P3** w.r.t. $y_i(t)$ is negative. If $Z_i(t) - y_i^*(t) > 0$, then, in time slot t the amount of energy demand being served is at least y_i^{max}, which is larger than the maximum amount of arrival ε_i during time slot t. Hence, the queue cannot increase, i.e., $Z_i(t+1) \leq Z_i(t) \leq V\alpha^{max} + \varepsilon_i$. If $Z_i(t) - y_i^*(t) \leq 0$, then $Z_i(t+1) \leq \varepsilon_i \leq V\alpha^{max} + \varepsilon_i$. Therefore, we have proved that $Z_i(t) \leq Z_i^{max}$.

   Finally, we prove $Q_i(t) + Z_i(t) \leq \Theta_i^{max}$ for every time slot t. Obviously, $Q_i(0) + Z_i(0) \leq \Theta_i^{max}$. Suppose $Q_i(t) + Z_i(t) \leq \Theta_i^{max}$ holds for time slot t. If $Q_i(t) + Z_i(t) \leq V\alpha^{max}$, then, according to the dynamics of $Q_i(t)$ and $Z_i(t)$, the maximum increase during one slot is $d_{i,2}^{max} + \varepsilon_i$. If $V\alpha^{max} < Q(t) + Z(t) \leq V\alpha^{max} + d_{i,2}^{max} + \varepsilon_i$, then LCMA will choose the maximum possible value for $y_i(t)$ since the partial derivative of the objective function in **P3** w.r.t. $y_i(t)$ is negative. Using the proof above, $Q_i(t+1)$ and $Z_i(t+1)$ cannot increase. Hence, $Q_i(t+1) + Z_i(t+1) \leq Q_i(t) + Z_i(t) \leq \Theta_i^{max}$. This completes the proof.
2. This follows directly from Lemma 3.1.

3. Once again, we prove the result by induction. When $t = 0$, $E_i(0) = 0 \leq E_i^{max}$. Now suppose that the bound above holds for time slot t. We need to show that it also holds for time slot $t + 1$. First, assuming that $0 \leq E_i(t) < \theta_i - V(\alpha^{max} + \beta_i^{max})$, then LCMA will choose the maximum value for $r_i(t)$ because the partial derivative of the objective function in **P3** w.r.t. $r_i(t)$ is always negative. Therefore, the battery would charge as much as possible, i.e., $0 \leq E_i(t) \leq E_i(t+1) < \theta_i - V(\alpha^{max} + \beta_i^{max}) + r_i^{max} \leq E_i^{max}$. Second, assuming that $\theta_i - V(\alpha^{max} + \beta_i^{max}) \leq E_i(t) \leq \theta_i - V(\alpha^{min} + \beta_i^{min})$, then the maximum charge and discharge rates for the battery are r_i^{max} and $-r_i^{min}$, respectively. Hence, $0 = \theta_i - V(\alpha^{max} + \beta_i^{max}) + r_i^{min} \leq E_i(t+1) \leq \theta_i - V(\alpha^{min} + \beta_i^{min}) + r_i^{max} \leq E_i^{max}$, where we have used the upper bound V_{max} of V. Third, suppose $\theta_i - V(\alpha^{min} + \beta_i^{min}) \leq E_i(t) \leq E_i^{max}$, then LCMA will choose the minimum value for $r_i(t)$ because the partial derivative of the objective function in **P3** w.r.t. $r_i(t)$ is always positive. Therefore, the battery would discharge as much as possible, i.e., $0 \leq \theta_i - V(\alpha^{min} + \beta_i^{min}) + r_i^{min} \leq E_i(t+1) \leq E_i(t) \leq E_i^{max}$. This completes the proof.
4. Since we choose our decisions to satisfy all constraints in **P3**, combining it with the results above together, all constraints of **P1** are satisfied. Therefore, our control decisions are feasible to **P1**.
5. As we have mentioned before, the LCMA is always trying to greedily minimize the R.H.S. of the upper bound (3.30) of the *drift-plus-penalty* term at every slot t over all possible feasible control policies including the optimal and stationary policy given in Theorem 3.1. Therefore, by plugging this policy into the R.H.S. of the inequality (3.30), we obtain the following:

$$\begin{aligned}
\triangle_V(t) \leq B &+ \sum_{i=1}^{N} \mathbb{E}\{(E_i(t) - \theta_i) r_i^{stat}(t) \mid \mathbf{K}(t)\} \\
&+ \sum_{i=1}^{N} \mathbb{E}\{Q_i(t)(d_{i,2}(t) - y_i^{stat}(t)) \mid \mathbf{K}(t)\} \\
&+ \sum_{i=1}^{N} \mathbb{E}\{Z_i(t)(\varepsilon_i - y_i^{stat}(t)) \mid \mathbf{K}(t)\} \\
&+ V\mathbb{E}\left\{ C_t\left(\sum_{i=1}^{N} g_i^{stat}(t)\right) + \sum_{i=1}^{N} F_i(r_i^{stat}(t)) \mid \mathbf{K}(t)\right\} \\
&\leq B + V \cdot \mathbf{P2}^* \leq B + V \cdot \mathbf{P1}^*,
\end{aligned}$$

where the following facts haven been used:

$$\begin{aligned}
\mathbb{E}\{r_i^{stat}(t) \mid \mathbf{K}(t)\} &= 0, \\
\mathbb{E}\{d_{i,2}(t) - y_i^{stat}(t) \mid \mathbf{K}(t)\} &\leq 0
\end{aligned}$$

$$\mathbb{E}\left\{C_t\left(\sum_{i=1}^{N} g_i^{stat}(t)\right) + \sum_{i=1}^{N} F_i(r_i^{stat}(t))\right\} = \mathbf{P2}^*,$$
$$\mathbb{E}\{\varepsilon_i - y_i^{stat}(t) \mid \mathbf{K}(t)\} \leq 0.$$

The first three facts follow from Lemma 3.1 and the last one follow from the second fact above with together $\varepsilon_i \leq \mathbb{E}\{d_{i,2}(t)\}$. Taking the expectation of both sides, using the law of iterative expectation, and summing over $t \in \{0, 1, 2, \ldots, T-1\}$, we have

$$V\mathbb{E}\left\{C_t\left(\sum_{i=1}^{N} g_i^{stat}(t)\right) + \sum_{i=1}^{N} F_i(r_i^{stat}(t))\right\}$$
$$\leq BT + VT \cdot \mathbf{P1}^* - \mathbb{E}\{L(T)\} + \mathbb{E}\{L(0)\}.$$

Dividing both sides by T, letting $T \to \infty$, and using the facts that $E\{L(0)\}$ are finite and $E\{L(t)\}$ are nonnegative, we arrive at the following performance guarantee:

$$\limsup_{T\to\infty} \frac{1}{T} \sum_{t=0}^{T-1} \sum_{i=1}^{N} \mathbb{E}\left\{C_t\left(\sum_{i=1}^{N} g_i^{stat}(t)\right) + \sum_{i=1}^{N} F_i(r_i^{stat}(t))\right\}$$
$$\leq \mathbf{P1}^* + B/V,$$

where $\mathbf{P1}^*$ is the optimal objective value, B is a constant, and V is a control parameter which has the maximum value given by (3.34).

3.5 Performance Evaluation

In this section, we provide numerical results based on real-world data sets to complement the analysis in the previous sections.

3.5.1 Simulation Setup

We consider a simple power system consisting of eight households in one neighborhood that share the same load serving entity and have on-site renewable generation, energy storage, and elastic and inelastic energy loads. The households are divided into two categories. For the first type of households (indexed by $i = 1, 2, 3, 4$), both the elastic and inelastic energy load arrivals during one slot are i.i.d. and take value from $[1, 5]$ kW-slot uniformly at random. For the second type of households (indexed by $i = 5, 6, 7, 8$), both the elastic and inelastic energy load arrivals during one slot are also i.i.d. and take value from $[1.5, 7.5]$ kW-slot uniformly at random.

For the renewable generation, we use the hourly average solar irradiance data for Los Angels area from the Measurement and Instrumentation Data center (MIDC) [10] at National Renewable Energy Laboratory. The period we consider in this paper is half year from January 1, 2011 to June 30, 2011. In total, this duration includes 181 days or 4344 1 h slots. The control interval is chosen to be 1 h. For different households, we use different scaling factors to characterize the heterogeneity of households. Specifically, we choose the scaling factors such that the average solar energy production during one slot is about 3 kW-slot for the first type of households and 4.5 kW-slot for the second type of households. We fix the maximum charge and discharge rates of batteries in households as follows: for $i \in \{1, 2, 3, 4\}$, $r_i^{max} = 1$ kW-slot, $r_i^{min} = -1$ kW-slot, and for $i \in \{5, 6, 7, 8\}$, $r_i^{max} = 1.5$ kW-slot, $r_i^{min} = -1.5$ kW-slot. Also, we choose $y_i^{max} = d_{i,2}^{max}$ for all i. The battery cost is assumed to be a simple quadratic function as follows:

$$F_i(r_i) = b_1 r_i^2,$$

where b_1 is a constant coefficient. For the purpose of simple illustration, we choose the same battery cost function for all households i in the evaluations.

For the LSE, we assume that the energy cost function is a smooth quadratic function as follows:

$$C_t(D) = c_1(t)D^2 + c_2 D + c_3.$$

where $c_1(t)$ is a time-varying coefficient used to model different electricity marginal costs across time slots while c_2 and c_3 are constant coefficients. In this evaluation, $c_1(t)$ takes value from $[0.1, 0.2]$ kW-slot uniformly at random, $c_2 = 0.1$, and $c_3 = 0.2$.

3.5.2 Results and Analysis

In order to analyze the performance improvement due to our LCMA, we compare it with the following two approaches.

- No storage, no demand response (B1): In this approach, households have no energy storage and do not differentiate between elastic and inelastic energy loads. The household tries to use the renewable energy as much as possible. When the renewable energy is not sufficient, the household draws energy from the utility grid. Unused renewable energy is wasted due to the lack of energy storage.
- Storage, no demand response (B2): In this approach, households have energy storage but do not consider demand response. The household uses renewable energy only as a supplement to the grid by consuming it whenever it is available. The household stores any extra renewable energy in its battery, but never charge the battery from the grid. The stored energy would be used to serve the future demands.

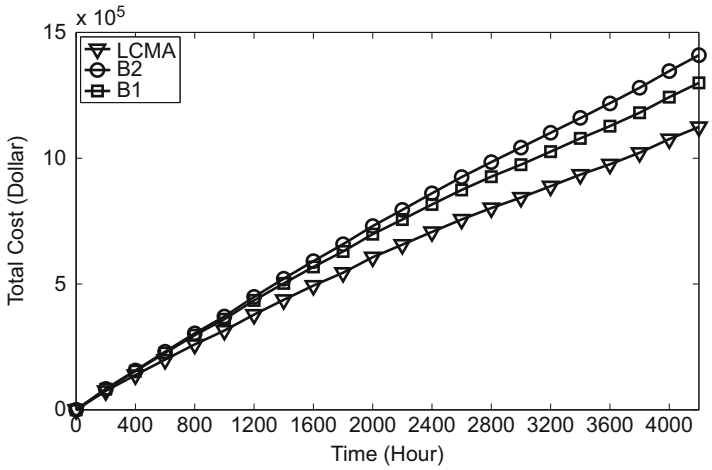

Fig. 3.2 Comparison of the total energy cost in three approaches

Note that LCMA differs from the approaches above in the sense that LCMA would actively charge the battery when the grid power is cheap while discharging it when the grid power is expensive. Moreover, LCMA differentiates between inelastic and elastic energy loads and delays the elastic energy loads to later time when the grid power cost is low.

In the first evaluation, we compare our algorithm with the two approaches above using the real-world solar power generation. Note that the performance of LCMA depends on the battery capacity, the battery cost, and the control parameters V and ε_i. We choose $b_1 = 0.5$, $E_i^{max} = 20\,\text{kW-slot}, i \in \{1, 2, 3, 4\}$, and $E_i^{max} = 30\,\text{kW-slot}, i \in \{5, 6, 7, 8\}$. The initial battery energy level at each household is chosen to be zero. Let $V = V^{max}$ and $\varepsilon_i = \mathbb{E}\{d_{i,2}\}, \forall i$. As can be seen in Fig. 3.2, our proposed LCMA can reduce the total energy cost by approximately 20% compared with B1 and 13% compared with B2 in the 6-month period. Also, the slopes of the lines are different, meaning that the savings are unbounded as the time increases.

In the following, we consider the impact of varying control parameters on the performance of LCMA.

- **Impact of Battery Capacity:** In this evaluation, we vary the battery capacities of households with other parameters fixed. We set $E_i^{max} = \{20, 30, 40\}\,\text{kW-slot}$ for $i \in \{1, 2, 3, 4\}$, $E_i^{max} = \{30, 40, 50\}\,\text{kW-slot}$ for $i \in \{5, 6, 7, 8\}$, and $V = V^{max}$. The result is illustrated in Fig. 3.3. From the figure, it is clear that the larger the capacity is, the more cost saving LCMA can obtain, which coincides with the algorithmic performance results of our algorithm in Theorem 3.2. As we have mentioned before, the saving comes from the fact that our algorithm would charge the battery when the marginal energy cost is low, while discharging it when the marginal energy cost is high.
- **Impact of Battery Cost:** Currently, the battery is still expensive. The charging or discharging operation would reduce the lifetime of the battery. However, it is

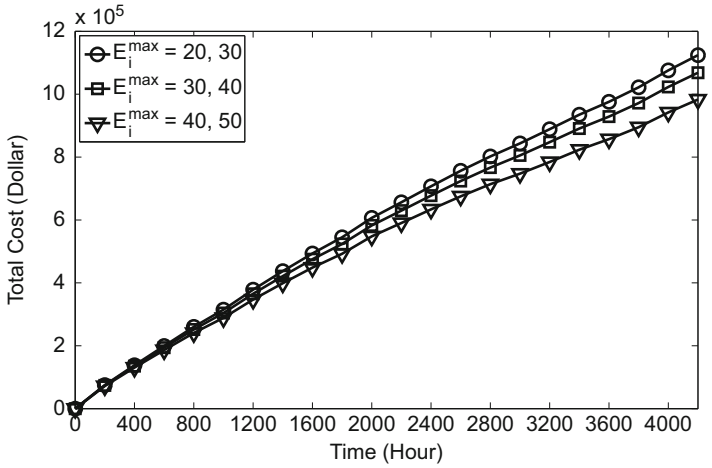

Fig. 3.3 The impact of battery capacity E_i^{max} on the cost saving

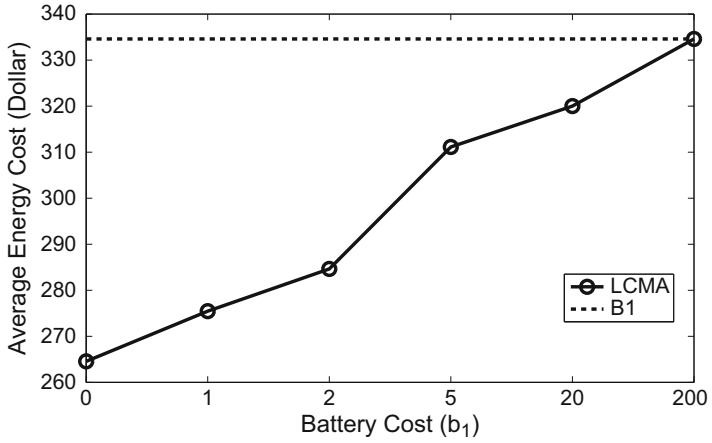

Fig. 3.4 The impact of battery cost b_1 on the cost saving

expected that the cost of battery would decrease greatly in the next decade. In this evaluation, we estimate the impact of battery cost on the cost saving of our algorithm. We set $b_1 = \{0, 1, 2, 5, 20, 200\}$ and keep $E_i^{max} = 20, i \in \{1, 2, 3, 4\}$, and $E_i^{max} = 30, i \in \{5, 6, 7, 8\}$ fixed. The result is shown in Fig. 3.4. Note that when the battery cost per usage during one-slot b_1 is very large (e.g., 200 \$), our algorithm would not charge or discharge the battery at all, so it is the same as the approach B1. As the battery cost increases, the total cost saving of LCMA compared with B1 would decrease until they are the same since the opportunity to utilize the temporal variation of electricity prices is smaller.

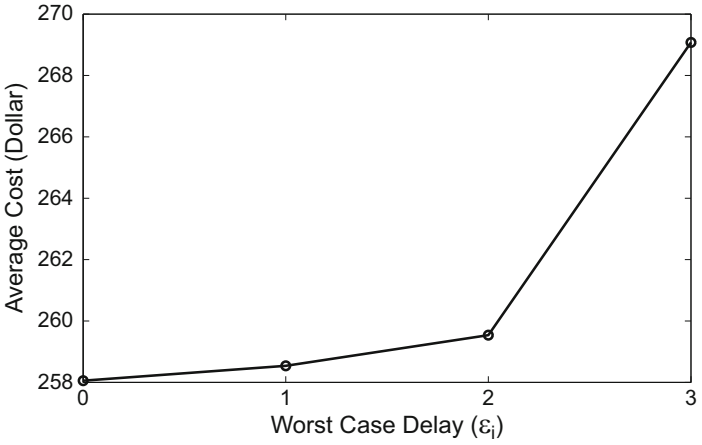

Fig. 3.5 The impact of ε_i on the cost saving

- **Impact of Worst-case Delay Requirement:** In this setting, we adjust the parameters ε_i while fixing other parameters to see the impact of the worst-case delay guarantee for elastic energy loads on the performance of LCMA. We choose $\varepsilon_i = \{0, 1, 2, 3\}, \forall i$, respectively. As observed in Fig. 3.5, the increase of ε_i (i.e., the worst-case delay) gives more opportunity to optimize the energy cost, since the elastic energy loads are more likely to be served in the low energy cost period.

Appendix

The Worst-case Delay for Buffered Elastic Loads

Here we prove Lemma 3.1.

Proof For all households i, consider any slot t for which $d_{i,2}(t) > 0$. We will show that this energy load $d_{i,2}(t)$ is served on or before time slot $t + \delta_i^{max}$ by contradiction. Suppose not, then during slots $\tau \in \{t+1, \ldots, t+\delta_i^{max}\}$, it must be that $Q_i(\tau) > 0$. Otherwise, the energy load $d_{i,2}(t)$ would have been served before τ. Therefore, $1_{Q(\tau)>0} = 1$, and from the update Eq. (3.25) of $Z_i(t)$, we have for all $\tau = \{t+1, \ldots, t+\delta_{max}\}$:

$$Z_i(\tau+1) \geq Z_i(\tau) - y_i(\tau) + \varepsilon_i.$$

Summing the above over $\tau = \{t+1, \ldots, t+\delta_i^{max}\}$ yields:

$$Z_i(t+\delta_i^{max}+1) - Z_i(t+1) \geq -\sum_{\tau=t+1}^{t+\delta_i^{max}} y_i(\tau) + \delta_i^{max}\varepsilon_i.$$

Rearranging the terms and using the facts that $Z_i(t+1) \geq 0$ and $Z_i(t+\delta_i^{max}+1) \leq Z_i^{max}$ yields:

$$\sum_{\tau=t+1}^{t+\delta_i^{max}} y_i(\tau) \geq \delta_i^{max}\varepsilon_i - Z_i^{max}. \tag{3.41}$$

Since the energy loads $d_{i,2}(t)$ are queued in a FIFO manner and $Q_i(t+1) \leq Q_i^{max}$, it would be served on or before time $t+\delta_i^{max}$ whenever there are at leat Q_i^{max} units of energy served during $\tau \in \{t+1, \ldots, t+\delta_i^{max}\}$. Since we have assumed that the energy loads $d_{i,2}(t)$ are not served by time $t+\delta_i^{max}$, it must be that $\sum_{\tau=t+1}^{t+\delta_i^{max}} y_i(\tau) < Q_i^{max}$. Comparing this inequality with (3.41) yields:

$$Q_i^{max} > \delta_i^{max}\varepsilon_i - Z_i^{max},$$

which implies that $\delta_i^{max} < (Q_i^{max} + Z_i^{max})/\varepsilon_i$, contradicting the definition of δ_i^{max} in (3.26).

References

1. Sean Barker, Aditya Mishra, David Irwin, Prashant Shenoy, and Jeannie Albrecht. Smartcap: Flattening peak electricity demand in smart homes. In *Proceedings of the IEEE International Conference on Pervasive Computing and Communications (PerCom)*, 2012.
2. M. J. Neely. *Stochastic Network Optimization with Application to Communication and Queueing Systems*. Morgan Claypool, 2010.
3. Leonidas Georgiadis, Michael J. Neely, and Leandros Tassiulas. *Resource allocation and cross-layer control in wireless networks*, volume 1. Now Publishers Inc., 2006.
4. Rahul Urgaonkar, Bhuvan Urgaonkary, Michael J. Neely, and Anand Sivasubramaniam. Optimal power cost management using stored energy in data centers. In *ACM International Conference on Measurement and Modeling of Computer Systems, SIGMETRICS 2011*, SAN JOSE, June 2011.
5. Dimitri P. Bertsekas. *Dynamic Programming and Optimal Control*. Athena Scientific, 2nd edition, 2000.
6. D. P. Bertsekas and J. N. Tsitsiklis. *Parallel and Distributed Compuation*. Old Tappan, NJ (USA); Prentice Hall Inc., 1989.
7. Stephen P. Boyd and Lieven Vandenberghe. *Convex optimization*. Cambridge University Press, 2004.
8. D.P. Palomar and M. Chiang. A tutorial on decomposition methods for network utility maximization. *Selected Areas in Communications, IEEE Journal on*, 24(8):1439–1451, 2006.
9. Privacy on the Smart Grid, IEEE Spectrum.
10. NREL: Measurement and Instrumentation Data Center.

Chapter 4
Risk-Constrained Optimal Energy Management for Smart Microgrids

4.1 System Model

Consider a microgrid consisting of CHP units, RES units, electrical storage (ES) units such as batteries, thermal storage (TS) units, heat boilers, power demand, and heat demand. In the microgrid, CHP units are deployed to increase the overall energy efficiency. Note that by generating heat and power simultaneously, the overall energy efficiency of CHP units can reach up to 80%, comparing with 33% efficiency of conventional thermal generation units [1]. In the microgrid, RES units such as wind turbines and solar panels are used to reduce carbon emissions. However, their power outputs are highly dependent on weather conditions, and thus are uncertain. This problem can be overcame by coordinating ES units with renewable energy source (RES) units. When the actual RES power outputs are different from the forecasted values, ES units are used to mitigate the imbalance by charging or discharging. Heat boilers and TS units in the microgrid can provide extra flexibility to CHP units by taking over the heat supply during low heat demand. The power demand in the microgrid is categorized into base load and deferrable load. Base load, also known as non-deferrable load, is the power demand that needs to be satisfied instantaneously at all times. Deferrable load is the power demand that is both interruptible and adjustable, and therefore has flexibility to be scheduled.

The microgrid is considered to be operated by the microgrid central controller that aims at minimizing the system operating costs by coordinating operation states of microgrid components. The microgrid is connected to the main grid through a distribution line. The bus that connected to the line is assumed to be the slack bus of the microgrid, where the connecting point is called the point of common coupling (PCC). The microgrid central controller makes decisions on purchasing and selling electricity from or to the electricity market based on information such as electricity

Y. Guo et al., *Stochastic Optimization for Distributed Energy Resources in Smart Grids*, SpringerBriefs in Electrical and Computer Engineering,
DOI 10.1007/978-3-319-59529-0_4

prices and RES power outputs. We set the operating time in the microgrid as discrete time slots, represented by t in our model, over T time slots, e.g, 1 day with 24 hourly time slots as the scheduling horizon. The list of notations used in this chapter is shown in Table 4.1.

4.1.1 Combined Heat and Power

Without loss of generality, we assume CHP units have been turned off for enough time before the operating day. Since the power output of each CHP unit has a upper and lower limit, we have:

$$\underline{P}_i I_{i,t} \leq p_{i,t} \leq \overline{P}_i I_{i,t}, \underline{Q}_i I_{i,t} \leq q_{i,t} \leq \overline{Q}_i I_{i,t}, \forall i, t. \tag{4.1}$$

Note that when CHP unit i is off, i.e., $I_{i,t} = 0$, both active and reactive power outputs of CHP unit i must be 0.

Additionally, the change of power outputs of CHP units between two consecutive time periods are constrained by ramping-up and ramping-down rates. When CHP unit i is started up at time t, i.e., $y_{i,t} = 1$, CHP unit i can generate at most $\overline{P}_i$ unit of energy in hour t. Similarly, we can formulate the ramping-down case. Therefore, we have following ramping-up and ramping-down constraints of CHP units:

$$p_{i,t} - p_{i,t-1} \leq \mathrm{RU}_i(1 - y_{i,t}) + \overline{P}_i y_{i,t}, \forall i, t \tag{4.2}$$

$$p_{i,t-1} - p_{i,t} \leq \mathrm{RD}_i(1 - z_{i,t}) + \overline{P}_i z_{i,t}, \forall i, t. \tag{4.3}$$

Besides, for each CHP unit i, we have following minimum-up and minimum-down time constraints:

$$\sum_{\tau=t}^{t+\mathrm{UT}_i-1} I_{i,\tau} \geq \mathrm{UT}_i y_{i,t}, \forall i, t \tag{4.4}$$

$$\sum_{\tau=t}^{t+\mathrm{DT}_i-1} (1 - I_{i,\tau}) \geq \mathrm{DT}_i z_{i,t}, \forall i, t. \tag{4.5}$$

The relationship between start-up and shut-down indicators $y_{i,t}$ and $z_{i,t}$ of CHP unit i is given as follows:

$$I_{i,t} - I_{i,t-1} = y_{i,t} - z_{i,t}, y_{i,t} + z_{i,t} \leq 1, \forall i, t. \tag{4.6}$$

Table 4.1 A list of notations

ρ^s	Probability of scenario s
ϵ	Confidence level
κ	Risk-aversion parameter
T	Number of time slots
$\mathrm{SU}_i/\mathrm{SD}_i$	Start-up/shut-down cost of CHP unit
$\mathrm{RU}_i/\mathrm{RD}_i$	Ramping-up/down rate limit of CHP unit
$\mathrm{UT}_i/\mathrm{DT}_i$	Minimum up/down time of CHP unit
$\overline{P}_i/\underline{P}_i$	Upper/lower limit of CHP unit active power output
$\overline{Q}_i/\underline{Q}_i$	Upper/lower limit of CHP unit reactive power output
α_i	Power-to-heat ratio of CHP unit
β_i/γ_i	Cost parameters of CHP unit
$G_{j,o}/B_{j,o}$	Real/imaginary part of microgrid admittance matrix
r_j/x_j	Resistance (reactance) of branch
$\overline{V}_j/\underline{V}_j$	Upper/lower limit of voltage magnitude
$\overline{\theta}_j/\underline{\theta}_j$	Upper/lower limit of voltage phase angle
$\overline{P}_{j,o}/\overline{Q}_{j,o}$	Maximum active/reactive line capacity between bus j and o
$\overline{P}_{g,t}/\overline{Q}_{g,t}$	Maximum allowable active/reactive power exchange between microgrid and main grid
$\pi_t^{\mathrm{DA},s}/\pi_t^{\mathrm{RT},s}$	Day-ahead/real-time market price
ψ_t	Cost parameter of electricity market
$\overline{d}_l/\underline{d}_l$	Upper/lower limit of deferrable load serving rate
D_l^s	Total energy consumption of deferrable load from start time to termination time
$T_l^{\mathrm{begin}}/T_l^{\mathrm{end}}$	Power consumption start/termination time of deferrable load
$P_{j,t}^b/Q_{j,t}^b$	Active/reactive power demand
$\overline{e}_k^+/\overline{e_k^-}$	Maximum charging/discharging rate of battery
$\overline{E}_k/\underline{E}_k$	Upper/lower limit of battery energy level
C_k^a	Degradation cost factor of battery
H_t	Heat demand
C_m^g	Generation cost factor of heat boiler
$\overline{h}_m$	Maximum heat output of heat boiler
$\overline{h}_u^+/\overline{h_u^-}$	Maximum charging/discharging rate of heat storage
$\overline{H}_u/\underline{H}_u$	Upper/lower limit of heat storage energy level
C_u^f	Degradation cost factor of heat storage
$I_{i,t}$	On/off status indicator of CHP unit
$y_{i,t}/z_{i,t}$	Start-up/shut-down indicator of CHP unit
$p_{i,t}^s/q_{i,t}^s$	Active/reactive power output of CHP unit
$w_{n,t}^s$	Active power output of RES unit
$d_{l,t}^s$	Serving rate of deferrable load
$V_{j,t}^s/\theta_{j,t}^s$	Voltage magnitude/phase angle
$P_{j,o}^{t,s}/Q_{j,o}^{t,s}$	Active/reactive power flow between bus j and o
$P_{j,t}^s/Q_{j,t}^s$	Active/reactive power injection at bus j
$p_{g,t}^{\mathrm{DA}}$	Day-ahead active power schedule between microgrid and the main grid
$p_{g,t}^{\mathrm{RT},s}/q_{g,t}^{\mathrm{RT},s}$	Real-time active/reactive power exchange between microgrid and the main grid

(continued)

Table 4.1 (continued)

ρ^s	Probability of scenario s
$e_{k,t}^{s,+}/e_{k,t}^{s,-}$	Charging/discharging power of battery
$E_{k,t}^s$	Stored electrical energy of battery
$h_{u,t}^{s,+}/h_{u,t}^{s,-}$	Charging/discharging heat of heat storage
$H_{u,t}^s$	Stored thermal energy of heat storage
$h_{m,t}^s$	Heat output of heat boiler
δ_t^s, ε^s, ζ	Auxiliary variables

4.1.2 Deferrable Load

In our model, deferrable load is the power demand that is both interruptible and adjustable such as charging of electric vehicles. The total energy requirement for a deferrable load D_l has to be served from the beginning time T_l^{begin} to the end time T_l^{end}. For each deferrable load, the load serving rate $d_{l,t}$ must be zero outside of the feasible operation interval. Deferrable load constraints are given as follows:

$$\sum_{l \in \mathcal{N}_j^l} d_{l,t} = D_l, \forall l, t \in [T_l^{\text{begin}}, T_l^{\text{end}}] \tag{4.7}$$

$$\underline{d}_l \leq d_{l,t} \leq \overline{d}_l, \forall l, t \in [T_l^{\text{begin}}, T_l^{\text{end}}] \tag{4.8}$$

$$d_{l,t} = 0, \forall l, t \notin [T_l^{\text{begin}}, T_l^{\text{end}}]. \tag{4.9}$$

4.1.3 Electrical and Thermal Storage

In our model, ES units such as batteries are used to mitigate power imbalances by charging or discharging appropriately. Each ES unit has a maximum charging and discharging rate. To avoid damage to the storage lifetime, the microgrid central controller needs to control ES units to operate within their upper and lower limits. Without loss of generality, we assume the ES energy level at the end of the operating day is the same as its initial energy level to ensure that each ES unit has the same capability in mitigating power imbalance for each day. The ES energy level difference between two consecutive time periods is caused by charging and discharging with different efficiencies. Therefore, we have following ES constraints:

$$0 \leq e_{k,t}^+ \leq \overline{e}_k^+, 0 \leq e_{k,t}^- \leq \overline{e}_k^-, \forall k, t \tag{4.10}$$

$$\underline{E}_k \leq E_{k,t} \leq \overline{E}_k, E_{k,1} = E_{k,T}, \forall k, t \tag{4.11}$$

$$E_{k,t+1} = E_{k,t} + \left(e_{k,t}^+ \eta_k^+ - \frac{e_{k,t}^-}{\eta_k^-} \right), \forall k, t. \tag{4.12}$$

Similarly, for TS units we have the following constraints:

$$0 \le h_{u,t}^{+} \le \overline{h}_{u}^{+}, 0 \le h_{u,t}^{-} \le \overline{h}_{u}^{-}, \forall u, t \tag{4.13}$$

$$\underline{H}_{u} \le H_{u,t} \le \overline{H}_{u}, H_{u,1} = H_{u,T}, \forall u, t \tag{4.14}$$

$$H_{u,t+1} = H_{u,t} + \left(h_{u,t}^{+} \eta_{u}^{+} - \frac{h_{u,t}^{-}}{\eta_{u}^{-}} \right), \forall u, t. \tag{4.15}$$

4.1.4 Heat Supply and Balance

In practice, the operation of CHP units is often heat-driven due to efficiency consideration. Since CHP units can generate heat and power simultaneously, we use a power-to-heat ratio α_i to represent the relationship between the power and heat outputs of CHP unit i. Note that when one unit of power is generated, CHP unit i generates α_i unit of useful heat. Heat outputs of CHP units coincide with power outputs serve part of the microgrid heat demand. Other thermal units such as heat boilers and heat storage units serve the remaining heat demand. The deployment of heat boilers and heat storage units provides extra flexibility to CHP units. For instance, during low heat demand, heat boilers and heat storage units may supply the total heat demand to allow CHP units to shut down, while during high heat demand, CHP units can be turned on to supply heat together with heat boilers and heat storage units. We define $\mathcal{N}_j^u$ as the set of heat storage units connected to bus j. We use heat storage units to store heat when there is a surplus of heat generation and supply heat when there is a lack of heat supply. For any scenario at any time, charging and discharging rates of heat storage units lie in a certain operating range. To avoid any overcharging or overdischarging, the microgrid central controller needs to control heat storage unit u to operate within upper and lower limits. We assume the heat storage unit energy level at the beginning of the operating day is the same as its initial energy level to maintain the same capability in mitigating heat imbalance for each day. The heat storage unit energy level difference between two consecutive time periods is caused by charging and discharging with different efficiencies. We further assume the microgrid heat demand belongs to the same heating zone. Note that this assumption can be easily extended to several heating zones [2]. Heat supply and demand constraints are given as follows:

$$\sum_{i \in \mathcal{N}_j^i} (\alpha_i p_{i,t}) + h_{m,t} + \sum_{u \in \mathcal{N}_j^u} \left(h_{u,t}^{-} - h_{u,t}^{+} \right) = H_t, \forall j, t \tag{4.16}$$

$$0 \le h_{m,t} \le \overline{h}_{m}, \forall m, t \tag{4.17}$$

4.1.4.1 Linearized Power Flow Equations

We use linearized power flow equations to model the microgrid power flow [3]. The following assumptions are made: (1) bus 0 is the slack bus which is connected to the main grid; (2) the square of the voltage magnitude difference of each bus j and bus 0 is approximately zero, i.e., $(V_{j,t} - V_{0,t})^2 \approx 0$; and (3) the difference of voltage phase angle across each branch (j, o) connecting bus j and bus o is sufficiently small so that $\sin(\theta_{j,t} - \theta_{o,t}) \approx \theta_{j,t} - \theta_{o,t}$, and $\cos(\theta_{j,t} - \theta_{o,t}) \approx 1$. We use $\mathcal{N}_j^i$, $\mathcal{N}_j^l$, $\mathcal{N}_j^n$ and $\mathcal{N}_j^k$ to denote sets of CHP units, deferrable loads, RES units, and batteries connected to bus j, respectively. Therefore, the net active and reactive power injection equations can be formulated as follows:

$$P_{0,t} = \sum_{i \in \mathcal{N}_0^i} p_{i,t} - p_t^{\mathrm{RT}} - \sum_{l \in \mathcal{N}_0^l} d_{l,t} - P_{0,t}^b + \sum_{n \in \mathcal{N}_0^n} w_{n,t} + \sum_{k \in \mathcal{N}_0^k} (e_{k,t}^- - e_{k,t}^+), \forall t \tag{4.18}$$

$$Q_{0,t} = \sum_{i \in \mathcal{N}_0^i} q_{i,t} - q_t^{\mathrm{RT}} - Q_{0,t}^b, \forall t \tag{4.19}$$

$$P_{j,t} = \sum_{i \in \mathcal{N}_j^i} p_{i,t} - \sum_{l \in \mathcal{N}_j^l} d_{l,t} - P_{j,t}^b + \sum_{n \in \mathcal{N}_j^n} w_{n,t} + \sum_{k \in \mathcal{N}_j^k} (e_{k,t}^- - e_{k,t}^+), \forall j \neq 0, t \tag{4.20}$$

$$Q_{j,t} = \sum_{i \in \mathcal{N}_j^i} q_{i,t} - Q_{j,t}^b, \forall j \neq 0, t. \tag{4.21}$$

Moreover, the net active and reactive power injections at other buses do not have power exchange with the main grid.

Similarly, we have following linearized power flow equations:

$$P_{j,t} = (2V_{j,t} - 1)G_{j,j} + \sum_{o(o \neq j)} G_{j,o}(V_{j,t} + V_{o,t} - 1) + B_{j,o}(\theta_{j,t} - \theta_{o,t}), \forall (j, o), t \tag{4.22}$$

$$Q_{j,t} = -(2V_{j,t} - 1)B_{j,j} + \sum_{o(o \neq j)} -B_{j,o}(V_{j,t} + V_{o,t} - 1) + G_{j,o}(\theta_{j,t} - \theta_{o,t}), \forall (j, o), t \tag{4.23}$$

$$P_{j,o}^t = G_{j,o}(V_{j,t} - V_{o,t}) + B_{j,o}(\theta_{j,t} - \theta_{o,t}), \forall (j, o), t \tag{4.24}$$

$$Q_{j,o}^t = B_{j,o}(V_{o,t} - V_{j,t}) + G_{j,o}(\theta_{j,t} - \theta_{o,t}), \forall (j, o), t. \tag{4.25}$$

4.1.4.2 Network Constraints

In the microgrid, voltage magnitude and phase angle at each bus are required to be in the safe operation interval. Therefore, we have upper and lower limits on voltage magnitude and phase angle as follows:

$$\underline{V}_j \leq V_{j,t} \leq \overline{V}_j, \underline{\theta}_j \leq \theta_{j,t} \leq \overline{\theta}_j, \forall j, t. \tag{4.26}$$

Besides, the network congestion is a major issue that needs to be considered. Hence, we have upper and lower limits on the active and reactive line flow as follows:

$$-\overline{P}_{j,o} \leq P^t_{j,o} \leq \overline{P}_{j,o}, -\overline{Q}_{j,o} \leq Q^t_{j,o} \leq \overline{Q}_{j,o}, \forall (j,o), t. \tag{4.27}$$

4.1.5 Electricity Market

Pool trading is commonly used in many electricity markets. Within a competitive electricity pool, supply and demand curves are built based on the bids received from sellers and buyers by a market operator. The intersection of these curves is the market clearing price. In our model, the microgrid is assumed to participate into a competitive pool-based two-settlement electricity market including a day-ahead forward market and a real-time spot market [4, 5]. The day-ahead electricity market is a financial market while the real-time electricity market is a physical market. The microgrid is considered to be a price-taker that does not have market power in either the day-ahead forward market or the real-time spot market.

The microgrid central controller needs to decide the amount of electricity bid into the day-ahead market, considering uncertainties in electricity prices and RES power outputs for the following operating day. In the afternoon on the day prior to the operating day, the day-ahead market is cleared by the market operator based on the day-ahead market clearing price. Because of the uncertainties in RES power outputs, the real-time power exchange may be different from the day-ahead power schedule between the microgrid and the main grid. The microgrid central controller needs to adjust the real-time power exchange based on the real-time RES power outputs to ensure the microgrid power balance. The market operator clears the real-time market and calculates payment for the microgrid based on the real-time market clearing price. Moreover, when the day-ahead power schedule is different from the real-time power exchange, a penalty also occurs. The market operator calculates the penalty payment based on the deviation between the day-ahead power schedule and the real-time power exchange.

To avoid the congestion on the line between the microgrid and the main grid, the active and reactive power passing through it must be kept below the capacity limits in each time. Therefore, we have following active and reactive power exchange capacity constraints:

$$-\overline{P}_t \leq p_t^{\mathrm{DA}} \leq \overline{P}_t, \forall t \tag{4.28}$$

$$-\overline{P}_t \leq p_t^{\mathrm{RT}} \leq \overline{P}_t, -\overline{Q}_t \leq q_t^{\mathrm{RT}} \leq \overline{Q}_t, t, \tag{4.29}$$

where $\overline{P}_t$ and $\overline{Q}_t$ represent the line capacity.

4.2 Problem Formulation

The problem of microgrid energy management with cogeneration and RES units is formulated as a two-stage stochastic program. Stochastic programming is a framework for solving optimization problems with uncertainties [6, 7]. In stochastic programming, uncertainties are modeled by scenarios. The constructed scenarios in our problem contain the information of all possible realizations of uncertainties in RES power outputs and electricity prices.

A two-stage stochastic optimization problem contains two stages of decisions. The first-stage decisions, also known as "here-and-now" decisions, must be done before the uncertainties are realized and thus do not depend on scenarios. The second-stage decisions, also known as "wait-and-see" decisions, are made after the uncertainties are disclosed. In our problem, the first-stage decision variables include unit commitment status of CHP units and power bids in the day-ahead electricity market. The second-stage decision variables include active and reactive power outputs of CHP units, heat outputs of heat boilers, charging and discharging decisions of batteries, load serving rates of deferrable loads, charging and discharging decisions of heat storage units, and power exchanges in the real-time market.

4.2.1 Conditional Value at Risk

In the proposed stochastic programming approach, the actual operating cost is a random variable, which may have a solution with a large operating cost under a high level of cost variability. A risk management scheme is needed to control the cost variability and choose the proper operating cost distribution considering the uncertainties associated with the RES power output and electricity prices. In our model, the risk of operating cost variability is considered through the CVaR approach. The CVaR at the ε confidence level can be defined as the expected operating cost larger than or equal to the $(1-\varepsilon)100\%$ scenarios that provides the highest operating cost, i.e., worst scenarios. Also, the $(1-\varepsilon)$–quantile of the operating cost distribution is known as value at risk (VaR), which is the minimum level of the operating cost that ensures the probability of obtaining a operating cost larger than that value is lower than $(1-\varepsilon)$, $\forall \varepsilon \in (0,1)$. A detailed description of the CVaR can be found in [8].

Constraint (4.30) allows incorporating the CVaR with the proposed stochastic approach. ζ is an auxiliary variable that represents the VaR, oc^s is the operating cost for scenario s, and ε^s is an auxiliary non-negative variable which equals to the difference between VaR and the oc^s when oc^s is larger than VaR, and equals to zero otherwise. Thus, we have:

$$\varepsilon^s \geq \text{oc}^s - \zeta, \varepsilon^s \geq 0, \forall s \tag{4.30}$$

4.2.2 Objective Function

The objective of the microgrid energy management problem is to minimize the expected microgrid operating cost and the risk, which can be written as follows:

$$\begin{aligned}
&\min \sum_i \sum_t (\text{SU}_i y_{i,t} + \text{SD}_i z_{i,t}) \\
&+ \sum_s \rho^s \sum_i \sum_t (\beta_i p_{i,t}^s + \gamma_i I_{i,t}) \\
&- \sum_s \rho^s \sum_t [p_t^{\text{DA}} \pi_t^{\text{DA},s} + (p_t^{\text{RT},s} - p_t^{\text{DA}}) \pi_t^{\text{RT},s} - \delta_t^s] \\
&+ \sum_s \rho^s \sum_m \sum_t C_m^g h_{m,t}^s \\
&+ \sum_s \rho^s \sum_k \sum_t C_k^a \left(\frac{e_{k,t}^{s,-}}{\eta_k^-} + e_{k,t}^{s,+} \eta_k^+ \right) \\
&+ \sum_s \rho^s \sum_u \sum_t C_u^f \left(\frac{h_{u,t}^{s,-}}{\eta_u^-} + h_{u,t}^{s,+} \eta_u^+ \right) \\
&+ \kappa \left(\zeta + \frac{1}{1-\epsilon} \sum_s \rho^s \varepsilon^s \right),
\end{aligned} \tag{4.31}$$

subject to constraint (4.1)–constraint (4.30).

Start-up costs and shut-down costs for CHP units over the operating day are shown in the first line of (4.31). The first term $\text{SU}_i y_{i,t}$ is the start-up cost for CHP unit i that incurs when CHP unit i starts up in time t, i.e., $y_{i,t} = 1$, while the second term $\text{SD}_i z_{i,t}$ is the shut-down cost for CHP unit i that incurs when CHP unit i shuts down in time t, i.e., $z_{i,t} = 1$.

In the second line of (4.31), we use a linear function $\beta_i p_{i,t}^s + \gamma_i I_{i,t}$ to represent operating costs for CHP units. The first term $\beta_i p_{i,t}^s$ shows the generation cost of CHP unit i in time t for scenario s while the second term $\gamma_i I_{i,t}$ describes the no-load cost of CHP unit i in time t. The no-load cost, also known as the minimum stable generation cost, incurs as long as CHP unit i is on, i.e., $I_{i,t} = 1$.

The third line of (4.31) represents the expected electricity market cost for the microgrid. In our formulation, the hourly bid that the microgrid submits to the day-ahead market is p_t^{DA}, while the hourly real-time power exchange between the microgrid and the main grid in the operating day is $p_t^{\mathrm{RT},s}$. When p_t^{DA} is positive/negative, the microgrid is selling/buying power to/from the day-ahead electricity market, and $p_t^{\mathrm{DA}}\pi_t^{\mathrm{DA},s}$ shows the revenue/cost of the microgrid by selling/buying electricity to/from the day-ahead electricity market in time t for scenario s. Similarly, when $\left(p_t^{\mathrm{RT},s}-p_t^{\mathrm{DA}}\right)$ is positive/negative, the microgrid is selling/purchasing power to/from the real-time electricity market, and $\left(p_t^{\mathrm{RT},s}-p_t^{\mathrm{DA}}\right)\pi_t^{\mathrm{RT},s}$ denotes the revenue/cost of the microgrid by selling/purchasing electricity to/from the real-time electricity market in time t for scenario s. We use auxiliary variable δ_t^s to denote the penalty that occurs when the real-time power exchange and the day-ahead power schedule are not the same, i.e., $\delta_t^s=\psi_t\left|p_t^{\mathrm{RT},s}-p_t^{\mathrm{DA}}\right|$.

In the fourth line of (4.31), we use a linear function $C_m^g h_{m,t}^s$ to capture the operating cost of heat boiler m in time t for scenario s. The term in the fifth line of (4.31), $C_k^a\left(e_{k,t}^{s,-}/\eta_k^- + e_{k,t}^{s,+}\eta_k^+\right)$, describes the degradation cost of battery k in time t for scenario s due to charging and discharging. Similarly, the term in the sixth line of (4.31), $C_u^f\left(h_{u,t}^{s,-}/\eta_u^- + h_{u,t}^{s,+}\eta_u^+\right)$, represents the degradation cost of heat storage unit u in time t for scenario s due to charging and discharging.

Finally, the last line of (4.31) is the CVaR multiplied by a risk-aversion parameter κ to show the relationship between the operating cost and the risk. When κ is equal to zero, the considered problem is risk-neutral. Moreover, the higher the value of κ, the more risk-averse the microgrid central controller is.

4.3 Solution Approach

We use a two-stage stochastic programming approach to solve uncertainties in RES power outputs and electricity prices. We assume the historic data for RES power outputs as well as day-ahead and real-time electricity prices can be obtained by the microgrid central controller. Furthermore, we assume uncertainties in electricity prices and RES power outputs are independent. However, uncertainties in the real-time and the day-ahead electricity market prices are dependent. We use the historic data to generate 133,225 scenarios with even probability. Each scenario contains the information of the hourly day-ahead and real-time electricity prices and the hourly RES power outputs in an operating day. We use a fast-forward scenario reduction method [9, 10] to reduce the original 133,225 scenarios into 100 scenarios. The objective of the scenario reduction is to obtain a small set of scenarios that can maintain properties of original scenarios at a reasonable level.

To solve the microgrid energy management problem with commercial solvers, the absolute term $\psi_t\left|p_t^{\mathrm{RT},s}-p_t^{\mathrm{DA}}\right|$ in the objective function (4.31) is transformed

into $\delta_t^s \geq \psi_t \left(p_t^{\mathrm{RT},s} - p_t^{\mathrm{DA}}\right)$ and $\delta_t^s \geq \psi_t \left(p_t^{\mathrm{DA}} - p_t^{\mathrm{RT},s}\right)$ by introducing an ancillary variable δ_t^s. Therefore, the microgrid energy management problem considering unit commitment of DER units, bidding strategy for electricity market, linearized AC power flow, and network constraints modeled in previous section is a large-scale mixed integer linear program (MILP), which can be directly solved by commercial solvers such as GUROBI 6.0.0 [11].

4.4 Case Study

4.4.1 Numerical Settings

The considered microgrid is tested on a modified IEEE 13-bus test feeder shown in Fig. 4.1 with three CHP units on bus 5, 6 and 10, one wind turbine on bus 8, one heat boiler on bus 3, six batteries on bus 1, 2, 5, 6, 9, 10, eleven heat storage units on bus $1-12$, eleven deferrable loads on bus $1-12$, and eleven base loads on bus $1-12$. Details about the original IEEE 13-bus test feeder can be found in [12]. The voltage regulator, switch and transformer in the original test feeder are replaced by distribution lines. The modified IEEE 13-bus test feeder is assumed to be a single-phase balanced network.

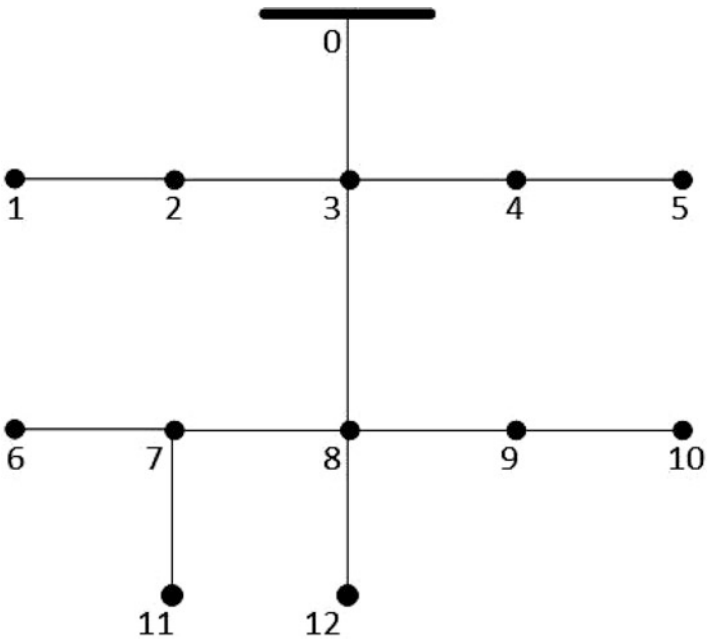

Fig. 4.1 Modified IEEE 13-bus test feeder

Table 4.2 Battery and heat storage unit parameters

$\underline{E}_k$ (kWh)	$\overline{E}_k$ (kWh)	$\overline{e}_k^+$ (kW)	$\overline{e}_k^-$ (kW)
40	180	100	100
$\underline{H}_u$ (kWh)	$\overline{H}_u$ (kWh)	$\overline{h}_u^+$ (kW)	$\overline{h}_u^-$ (kW)
100	250	100	100

We assume the power and heat demand can be perfectly forecasted. To run the simulation, we use the historic data for wind power [13], total power demand [7], day-ahead and real-time electricity prices [14] with appropriate scaling coefficients for the forecasts. Base load is set to be 90% of the power demand. Deferrable load is set to be 10% of the power demand. The data of impedance of each branch in the test feeder are from [15]. Parameters of CHP units in the microgrid are from [16]. Parameters of each identical battery, and each identical heat storage unit in the microgrid are given in Table 4.2, respectively. CHP units and the heat boiler in the microgrid are all natural gas-fueled generating units. The electricity market penalty factor ψ_t is 0.07\$/kWh. The maximum active and reactive power exchanges with the main grid are set to be 5000 kW and 5000 kVAR, respectively. The generation cost factor of heat boiler is set as 0.0205\$/kWh. The power-to-heat ratio is set to be identical for CHP units as 1.1. The maximum heat output of the heat boiler is 6000 kW. Degradation cost factors for each battery and each heat storage unit are 0.00027\$/kWh and 0.00034\$/kWh, respectively. The base values of apparent power and voltage magnitude are set to be 5000 kVA and 4.16 kV, respectively.

All simulations are implemented on a desktop computer with 3.4 GHz Intel Core i7-4770 CPU and 8GB RAM.

4.4.2 Simulation Results

4.4.2.1 Stochastic Approach Versus Deterministic Approach

We first compare our approach with a deterministic approach in solving the microgrid energy management problem. In this comparison, we consider uncertainties in both wind power output and the electricity prices. We compare these two approaches by changing the wind penetration level from 0% to 25%. The wind penetration level is defined as the average wind power output divided by the average total load demand. For the deterministic approach, we use historic data for the wind power output and electricity prices of one operating day. Figure 4.2 shows the simulation result that the microgrid expected operating cost decreases as the wind penetration level increases for both approaches. This is reasonable because the microgrid expected operating cost will be lower if the wind penetration level is higher since the wind turbine is assumed to have no generation cost. Moreover, we also observe that the microgrid expected operating cost reduces faster when using stochastic approach. Therefore, simulation results confirm that the stochastic approach is more capable in handling uncertainties than the deterministic approach.

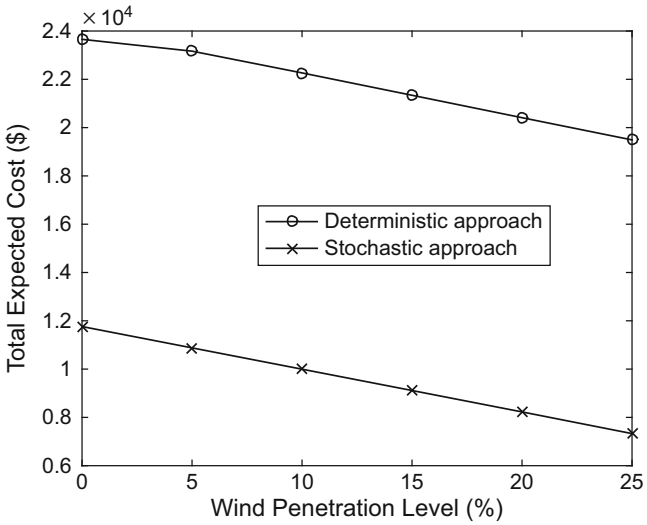

Fig. 4.2 The microgrid expected operating cost with different wind penetration levels using stochastic approach and deterministic approach

4.4.2.2 Expected Operating Cost and CVaR

In our proposed framework, there are two risk parameters κ and ϵ. In this comparison, we discuss how these parameters affect the CVaR and the microgrid expected operating cost. We compare these two values by change the risk-aversion parameter κ from 0 to 2 with the wind penetration level set to 25% and ϵ set to 0.79 and 0.99, respectively. The simulation is conducted using the reduced 100 scenarios. As shown in Figs. 4.3 and 4.4, the CVaR decreases and the expected operating cost increases simultaneously with the increase of the risk-aversion parameter, respectively. It is reasonable since the increase of the value of κ would increase the relative importance of the risk term. Moreover, due to the changing trade-off between the microgrid expected operating cost and the CVaR, we have that larger κ results in a higher expected operating cost and a lower CVaR. Furthermore, larger ϵ value means more conservative decisions. Thus, increasing the parameters κ and ϵ implies a higher level of risk-aversion.

4.4.2.3 Voltage Regulation Tests

The power quality is one of the concerns in microgrid energy management including voltage magnitude and phase angle. Figures 4.5 and 4.6 show the voltage magnitude and phase angle at each bus in the microgrid, respectively. It can be observed that the voltage magnitude and phase angle at each bus are in the safe operation interval. Therefore, the power quality of our proposed model is ensured.

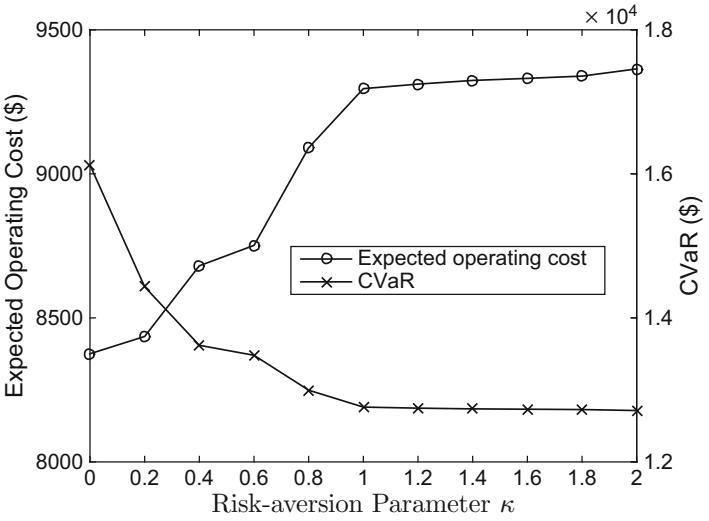

Fig. 4.3 The microgrid expected operating cost and the CVaR with different risk-aversion parameters

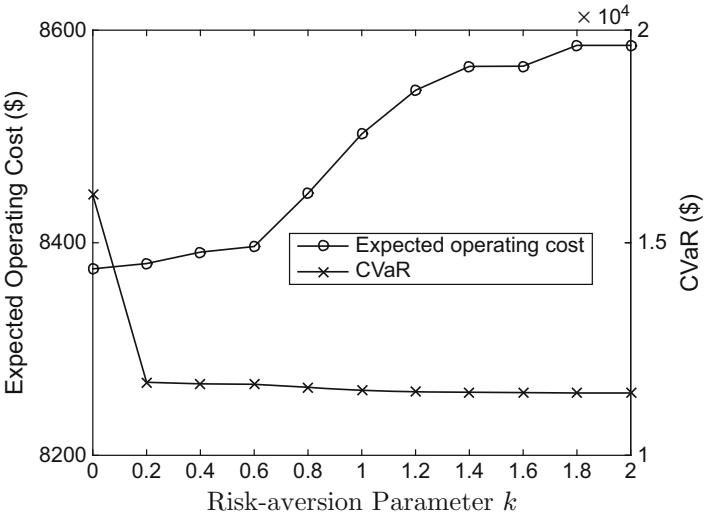

Fig. 4.4 The microgrid expected operating cost and the CVaR with different risk-aversion parameters

4.4.2.4 Sensitivity Analysis

In this section, we do the sensitivity analysis to observe the performance of the stochastic approach in solving the microgrid energy management problem with

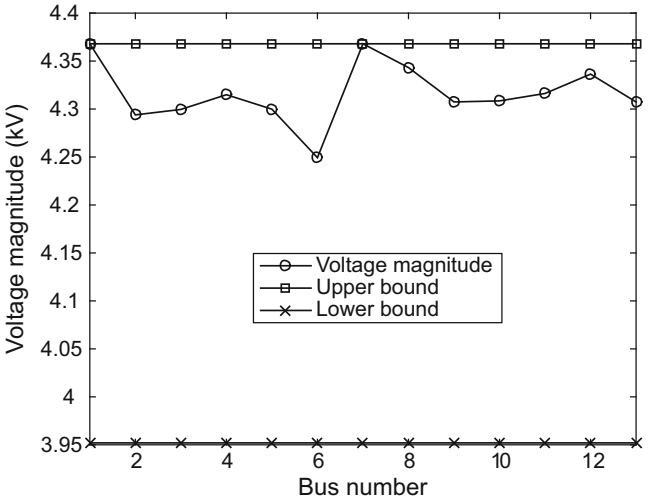

Fig. 4.5 The voltage magnitude of each bus in the microgrid

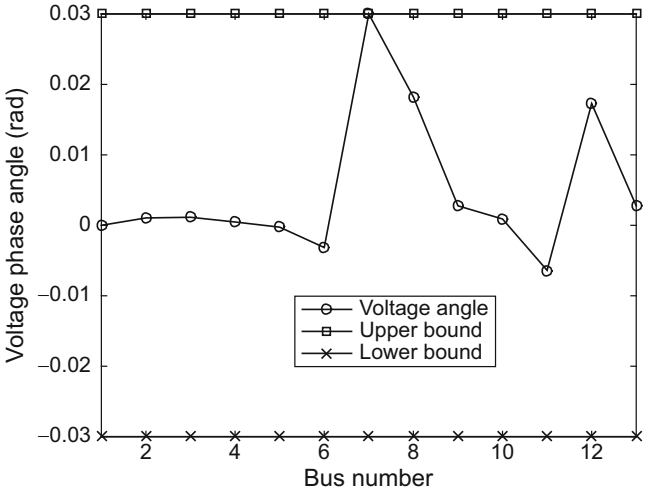

Fig. 4.6 The voltage phase angle of each bus in the microgrid

cogeneration and RES units. We check the influences on the microgrid energy management performance when changing the deferrable load serving time interval in two scenarios: with or without batteries. The impact of the deferrable load time interval on the microgrid expected operating cost is shown in Fig. 4.7. It can be observed that in scenario one, the microgrid has lower expected operating cost than that of scenario two. This is reasonable because in scenario one, batteries and the deferrable load are utilized together to reduce the power imbalance. Besides, as the

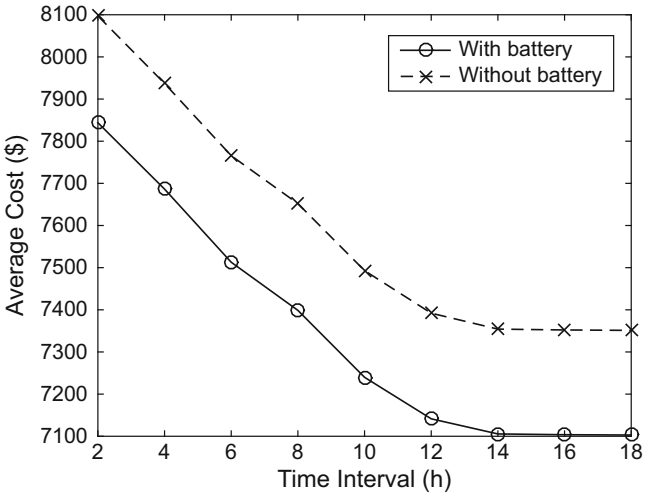

Fig. 4.7 The microgrid expected operating costs with different deferrable load serving time intervals

length of deferrable load serving time interval increases, the microgrid expected operating cost reduces. The reason is that the scenario with longer deferrable load time interval has more flexibility.

References

1. *Efficiency Benefits*.
2. Miguel C. and J. Arroyo M. A computationally efficient mixed-integer linear formulation for the thermal unit commitment problem. *Power Systems, IEEE Transactions on*, 21(3): 1371–1378, August 2006.
3. Mohammad E. Khodayar, Masoud Barati, and Mohammad Shahidehpour. Integration of high reliability distribution system in microgrid operation. *Smart Grid, IEEE Transactions on*, 3(4):1997–2006, December 2012.
4. Mohammad Tasdighi, Hassan Ghasemi, and Ashkan Rahimi-Kian. Residential microgrid scheduling based on smart meters data and temperature dependent thermal load modeling. *Smart Grid, IEEE Transactions on*, 5(1):349–357, 2014.
5. Masood Parvania, Mahmud Fotuhi-Firuzabad, and Mohammad Shahidehpour. Optimal demand response aggregation in wholesale electricity markets. *Smart Grid, IEEE Transactions on*, 4(4):1957–1965, December 2013.
6. Ali T Al-Awami and Eric Sortomme. Coordinating vehicle-to-grid services with energy trading. *Smart Grid, IEEE Transactions on*, 3(1):453–462, 2012.
7. Jianhui Wang, Mohammad Shahidehpour, and Zuyi Li. Security-constrained unit commitment with volatile wind power generation. *Power Systems, IEEE Transactions on*, 23(3):1319–1327, August 2008.
8. R Tyrrell Rockafellar and Stanislav Uryasev. Optimization of conditional value-at-risk. *Journal of risk*, 2:21–42, 2000.

9. Jitka Dupačová, Nicole Gröwe-Kuska, and Werner Römisch. Scenario reduction in stochastic programming. *Mathematical programming*, 95(3):493–511, 2003.
10. Ehsan Hajipour, Mokhtar Bozorg, and Mahmud Fotuhi-Firuzabad. Stochastic capacity expansion planning of remote microgrids with wind farms and energy storage. *Sustainable Energy, IEEE Transactions on*, 6(2):491–498, April 2015.
11. *GUROBI*, 2015 (accessed February 3, 2015).
12. *Distribution Test Feeders*.
13. *National Wind Technology Center M2 Tower*, 2015 (accessed February 3, 2015).
14. *PJM - Markets and Operations*, 2015 (accessed February 3, 2015).
15. Hung D Nguyen and Konstantin Turitsyn. Voltage multi-stability in distribution grids with power flow reversal. *arXiv preprint arXiv:1404.6581*, 2014.
16. SX Chen, Hoay Beng Gooi, and MingQiang Wang. Sizing of energy storage for microgrids. *Smart Grid, IEEE Transactions on*, 3(1):142–151, March 2012.

Chapter 5
Conclusion

5.1 Concluding Remarks

Driven by the benefits of increased energy efficiency, reduced carbon emissions, and improved power quality and reliability, DERs including renewable and distributed generation, distributed storage, and smart loads are envisioned to be an integral part of emerging smart grids. Yet managing potentially large numbers of DERs presents significant challenges for system operators due to their distributed and uncertain nature. By leveraging pervasive communication, computation, and control technologies in smart grids, it becomes possible to aggregate and coordinate DERs to improve system operations.

Motivated by these facts, we constructed a hierarchical resource management framework to integrate large numbers of DERs based on a variety of approaches to cope with resource uncertainty and complexity in this brief. Specifically, we first proposed a three-level hierarchical architecture for the coordinated management of DERs. Under this architecture, resource management algorithms to coordinate DERs at the three levels—home level, neighborhood level, and microgrid level—have been developed, respectively. Optimization problems taken into account the resource uncertainties and unique characteristics of each level have been formulated, and efficient algorithms based on stochastic optimization were developed to solve these problems. The effectiveness and efficiency of these algorithms have been theoretically analyzed and/or numerically tested using real-world data set. The work presented in this book will improve the operation of future cyber-physical energy systems that face resource uncertainty and complexity.

Y. Guo et al., *Stochastic Optimization for Distributed Energy Resources in Smart Grids*, SpringerBriefs in Electrical and Computer Engineering,
DOI 10.1007/978-3-319-59529-0_5

5.2 Future Work

In the future, we plan to extend our work to two directions. First, we plan to extend the framework to consider the impact of DERs in transmission networks. In particular, the implications of DERs to transmission network operation and planning will be modeled and analyzed in a comprehensive manner. Second, in addition to stochastic optimization, we will explore other optimization methods under uncertainty such as robust optimization and data-driven optimization to study the DER management problem and develop corresponding algorithms.